



Contents lists available at ScienceDirect

Journal of Rock Mechanics and Geotechnical Engineering

journal homepage: www.jrmge.cn

Review

Numerical simulations of supercritical carbon dioxide fracturing: A review

Lin Wu^{a,b,*}, Zhengmeng Hou^{a,**}, Zhifeng Luo^b, Ying Xiong^a, Nanlin Zhang^b, Jiashun Luo^a, Yanli Fang^a, Qianjun Chen^a, Xuning Wu^a

^a Institute of Subsurface Energy Systems, Clausthal University of Technology, Clausthal-Zellerfeld, 38678, Germany

^b State Key Laboratory of Oil and Gas Reservoir Geology and Exploitation, Southwest Petroleum University, Chengdu, 610500, China

ARTICLE INFO

Article history:

Received 28 March 2022

Received in revised form

9 June 2022

Accepted 14 August 2022

Available online 28 September 2022

Keywords:

Wellbore

Fracturing

Proppant transport

Supercritical carbon dioxide

Fracture initiation and propagation

ABSTRACT

As an emerging waterless fracturing technology, supercritical carbon dioxide (SC-CO₂) fracturing can reduce reservoir damage and dependence on water resources, and can also promote the reservoir stimulation and geological storage of carbon dioxide (CO₂). It is vital to figure out the laws in SC-CO₂ fracturing for the large-scale field implementation of this technology. This paper reviews the numerical simulations of wellbore flow and heat transfer, fracture initiation and propagation, and proppant transport in SC-CO₂ fracturing, including the numerical approaches and the obtained findings. It shows that the variations of wellbore temperature and pressure are complex and strongly transient. The wellhead pressure can be reduced by tubing and annulus co-injection or adding drag reducers into the fracturing fluid. Increasing the temperature of CO₂ with wellhead heating can promote CO₂ to reach the well bottom in the supercritical state. Compared with hydraulic fracturing, SC-CO₂ fracturing has a lower fracture initiation pressure and can form a more complex fracture network, but the fracture width is narrower. The technology of SC-CO₂ fracturing followed by thickened SC-CO₂ fracturing, which combines with high injection rates and ultra-light proppants, can improve the placement effect of proppants while improving the complexity and width of fractures. The follow-up research is required to get a deeper insight into the SC-CO₂ fracturing mechanisms and develop cost-effective drag reducers, thickeners, and ultra-light proppants. This paper can guide further research and promote the field application of SC-CO₂ fracturing technology.

© 2023 Institute of Rock and Soil Mechanics, Chinese Academy of Sciences. Production and hosting by Elsevier B.V. This is an open access article under the CC BY-NC-ND license (<http://creativecommons.org/licenses/by-nc-nd/4.0/>).

1. Introduction

Hydraulic fracturing proposed in 1947 (Montgomery and Smith, 2010) has made significant contributions to oil-and-gas industry (Barbati et al., 2016; Wei et al., 2020). However, as the exploration and development mainstream gradually change from conventional oil-and-gas resources to unconventional ones such as shale oil, shale gas, and coalbed methane (Gale et al., 2014; Mojidi et al., 2021), the disadvantages of hydraulic fracturing gradually appear in view of further implementations. Since the development of

unconventional oil-and-gas resources often requires volume fracturing with high water consumption (Estrada and Bhamidimarri, 2016), it is hardly applicable in areas with water shortages. In addition, hydraulic fracturing is easy to cause the expansion of clay minerals and reduce the matrix permeability (Khan et al., 2021). As there are still a lot of residues in the fracture due to incomplete flowback, the fracturing productivity can be seriously deteriorated (Chen et al., 2019). Finally, a large volume of fracturing flowback fluid with high turbidity and chemical oxygen content is difficult to treat, causing environmental pollution (Lester et al., 2015; Mohammad et al., 2018).

Mitigating the aforementioned disadvantages brought waterless or lower-water fracturing technologies into focus, such as hydrocarbon fracturing, liquid nitrogen fracturing, high-energy gas fracturing, and self-propping fracturing (Li et al., 2021a; Mojidi et al., 2021). In hydrocarbon fracturing, liquefied petroleum gas, liquefied natural gas, or N-Heptane are usually used as fracturing fluids,

* Corresponding author. Institute of Subsurface Energy Systems, Clausthal University of Technology, Clausthal-Zellerfeld, 38678, Germany.

** Corresponding author.

E-mail addresses: lin.wu@tu-clausthal.de (L. Wu), hong@tu-clausthal.de (Z. Hou).

Peer review under responsibility of Institute of Rock and Soil Mechanics, Chinese Academy of Sciences.

which are flammable or explosive, thus the safety risk increases (Schwartz, 2016; Liew et al., 2020; Mehmood et al., 2021). In liquid nitrogen fracturing, the ultra-low temperature will cause great damage to the steel pipes, thus glass fibers are required. This can greatly increase the fracturing costs (Huang et al., 2020; Ali et al., 2022). Moreover, the fracture length is short in high-energy gas fracturing, and fractures cannot be propped, leading to a limited stimulation effect (Jaimes et al., 2012). Similarly, self-propping fracturing also has some marked shortcomings. For example, the phase state of fracturing fluid cannot be ideally transformed, and leaked fracturing fluid may cause the blockage of matrix pore (Luo et al., 2020; Zhang et al., 2022). Therefore, further development of these waterless or lower-water fracturing technologies is needed.

As an inert gas, carbon dioxide (CO₂) is non-flammable and non-explosive, and pure CO₂ is non-corrosive (Mitu et al., 2017), thus CO₂ fracturing can effectively avoid the aforementioned problems. According to the phase state of CO₂ in the fracture, CO₂ fracturing can be specifically divided into liquid carbon dioxide (L-CO₂) fracturing and supercritical carbon dioxide (SC-CO₂) fracturing (Gupta and Bobier, 1998; Brown, 2000). SC-CO₂ has dual properties of liquid and gas, i.e. high density and diffusion coefficient, low viscosity and surface tension (Sihvonen et al., 1999; Nikolai et al., 2019), thus SC-CO₂ fracturing can achieve a better stimulation effect than L-CO₂ fracturing (Ishida et al., 2012). SC-CO₂ fracturing has unique advantages in reducing reservoir damage and water resource dependence (Wang et al., 2012, 2015; Li et al., 2021b), as well as some additional advantages. Firstly, CO₂ has a good energy-enhancing effect, fast and complete flowback after fracturing, and the flowback fluid is easy to treat (Liu et al., 2014; Wang et al., 2019a). Secondly, the characteristics of high diffusion coefficient and low viscosity are conducive to the flow of SC-CO₂ and can reduce pressure loss, which is more favorable to form complex fracture networks (Inui et al., 2014; Memon et al., 2022). Thirdly, the high filtration of SC-CO₂ fracturing fluid results in a lower fracture initiation pressure than in hydraulic fracturing, thus reducing the fracturing difficulty (Bennour et al., 2015; Luo et al., 2021a). Furthermore, SC-CO₂ can dissolve in crude oil to reduce viscosity, replace methane adsorbed on the rock surface or react with hydrogen to generate methane (Cao et al., 2022; Luo et al., 2022a; Xiong et al., 2022), improve oil-and-gas reservoir recovery, realize permanent geological storage of CO₂, and mitigate the greenhouse effect (Middleton et al., 2015). Therefore, SC-CO₂ fracturing is more promising in the development of unconventional reservoirs compared with other waterless or lower-water fracturing technologies (Middleton et al., 2015).

As an emerging fracturing technology, SC-CO₂ fracturing has been theoretically and numerically investigated, promoting its field implementation. The paper tries to review the numerical simulations of wellbore flow and heat transfer, fracture initiation and propagation, and proppant transport in SC-CO₂ fracturing. Then, the limitations of the numerical simulations in SC-CO₂ fracturing and the directions of the follow-up research are substantiated and outlined.

2. Numerical approaches to SC-CO₂ fracturing

2.1. Numerical approaches to wellbore flow and heat transfer

The key to the successful implementation of SC-CO₂ fracturing technology is that CO₂ reaches the well bottom in the supercritical state (Cheng et al., 2014; Wu and Luo, 2022). The accurate prediction of wellbore temperature and pressure directly affects the judgment of the phase state of CO₂. Since the SC-CO₂ fracturing technology is proposed, many numerical simulations of wellbore flow and heat transfer in SC-CO₂ fracturing have been carried out,

as shown in Table A1. It can be observed that previous simulations are mainly focused on vertical wells and consider different fracturing technologies: tubing fracturing, tubing and annulus co-injection fracturing, and coiled tubing jet fracturing. The differences among these three fracturing technologies are illustrated in Fig. 1.

In terms of wellbore flow and heat transfer state, previous simulations mainly include three types: (i) unsteady flow and heat transfer, (ii) steady flow and heat transfer, and (iii) steady flow and unsteady heat transfer. The unsteady flow and heat transfer are dominant because they can better describe the complex process of flow and heat transfer in the wellbore. Still, the respective calculation process is coupled with temperature, pressure, and physical properties, which significantly increases the computational workload. In terms of describing the heat transfer between CO₂ and formation rock, there are two main modes: overall description and separate description. The overall description aims to establish the comprehensive heat transfer coefficient or comprehensive thermal resistance. In contrast, the separate description establishes the differential equation for each heat transfer medium. The latter is more suitable for mechanism research because it can describe the temperature variation process of each heat transfer medium. Therefore, the latter is widely used, but it has more computational workload than the former.

In the process of wellbore flow, CO₂ is subjected to gravity, friction, and pressure. The calculation of friction directly affects the prediction of wellbore pressure, thus selection of the friction coefficient model is quite important. The model proposed by Chen (1979) suitable for all roughness values and Reynolds numbers, as shown in Eq. (1), was widely adopted to calculate friction coefficient in previous simulations. Moreover, Span-Wagner (S-W) state equation and Fenghour-Vesovic (F-V) transport equation, especially applicable to CO₂, were adopted in all models. The S-W state equation uses Helmholtz's free energy to calculate the state properties of CO₂, such as density and heat capacity. The applicable temperature ranges from the three-phase point temperature to 1100 K, while the pressure ranges from the three-phase point pressure to 800 MPa (Span and Wagner, 1996). The F-V transport equation, adopted to calculate viscosity and thermal conductivity, has an error of less than 0.3% under normal temperature and pressure, less than 3.6% under medium and low pressure, and no more than 5% under high pressure (Fenghour et al., 1998).

$$\frac{1}{\sqrt{f}} = -2\log_{10} \left\{ \frac{\Delta/d}{3.7065} - \frac{5.0452}{Re} \log_{10} \left[\frac{(\Delta/d)^{1.1098}}{2.8257} \right] + \frac{5.8506}{Re^{0.8981}} \right\} \quad (1)$$

where f is the friction coefficient, Δ is the tubing roughness, d is the inner diameter of tubing, and Re is the Reynolds number.

In the process of wellbore heat transfer, there are mainly three types of heat sources: friction heat, Joule-Thomson effect, and expansion/compression work. Friction heat can be ignored only when the injection rate is abnormally low (Guo and Zeng, 2015; Li et al., 2018a; Lyu et al., 2018a), and ignoring friction heat will underestimate bottom hole temperature (BHT) and overestimate bottom hole pressure (BHP) when the injection rate is high. Moreover, BHT will be overestimated if friction heat is only regarded as being absorbed by CO₂ (Yang et al., 2018a; Wu et al., 2021). Joule-Thomson effect has a minor impact on wellbore temperature and pressure, which can be ignored within the scope of the engineering (Li et al., 2018a; Yang et al., 2018a). When the pressure gradient in the wellbore changes from positive value to negative value, the impact of Joule-Thomson effect on temperature will also change from heating to cooling (Lyu et al., 2018a). Finally, the

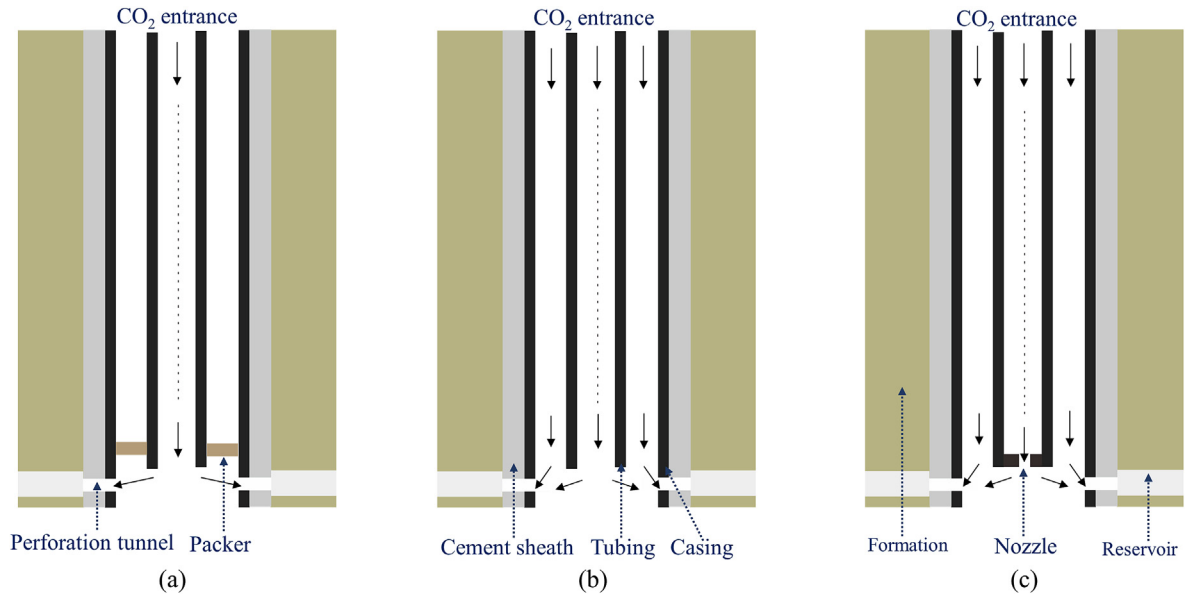


Fig. 1. Comparison of the three fracturing technologies: (a) Tubing fracturing; (b) Tubing and casing co-injection fracturing; and (c) Coiled tubing jet fracturing.

impact of expansion/compression work on wellbore heat transfer and flow under low and high injection rates cannot be ignored (Li et al., 2018a). The heat transfer equation considering all heat sources is shown in Eq. (2), in which the last three terms are friction heat, expansion/compression work, and Joule-Thomson effect, respectively (Li et al., 2018a). The effects of heat sources on BHT and BHP under different injection rates are depicted in Fig. 2:

$$\frac{dT_t}{dz} + \frac{\pi U d}{q_c c_c} T_t = \frac{\pi U d}{q_c c_c} T_{ei} + \frac{1}{c_c \rho_c} \frac{dp_{fr}}{dz} + \frac{1}{c_c \rho_c} \frac{dp_t}{dz} + \alpha_j \frac{dp_t}{dz} \quad (2)$$

where T_t is the temperature of CO₂ in the tubing; z is the vertical depth; U is the total heat transfer coefficient; q_c is the mass flow rate of CO₂ in the tubing; c_c is the heat capacity of CO₂ in the tubing; T_{ei} is the initial formation temperature; ρ_c is the density of CO₂ in the tubing; p_{fr} is the flow friction resistance; p_t is the pressure of CO₂ in the tubing; and α_j is the Joule-Thomson coefficient.

In addition, there are mainly two types of heat transfer media: CO₂, tubing, annulus, casing, cement sheath, and formation (CTACSF); CO₂, annulus, cement sheath, and formation (CASF). Dou et al. (2013), Cheng et al. (2014) and Lv et al. (2015) suggested that the temperature decrease induced by tubing and casing could be ignored in engineering practice considering the large thermal conductivity and thin wall thickness of tubing and casing. Furthermore, the effects of vertical heat conduction and natural convection in annulus and cement sheath on the prediction results of wellbore temperature in SC-CO₂ fracturing are further clarified. Specifically, the effect of axial heat conduction of fluid on temperature is negligible (Gong et al., 2019a). Natural convection heat transfer in the annulus can increase BHT, but this effect is very small and negligible (less than 0.5 °C) (Lyu et al., 2018a). The heat conduction of cement sheath strongly impacts the wellbore temperature, and ignoring it will seriously overestimate BHT (Yi et al., 2019).

In order to accurately predict temperature, pressure, and phase state of CO₂, and reduce computational workload, it is necessary to choose a suitable model according to the site-specific problems, or to establish a new model considering different heat sources, and heat transfer media, etc.

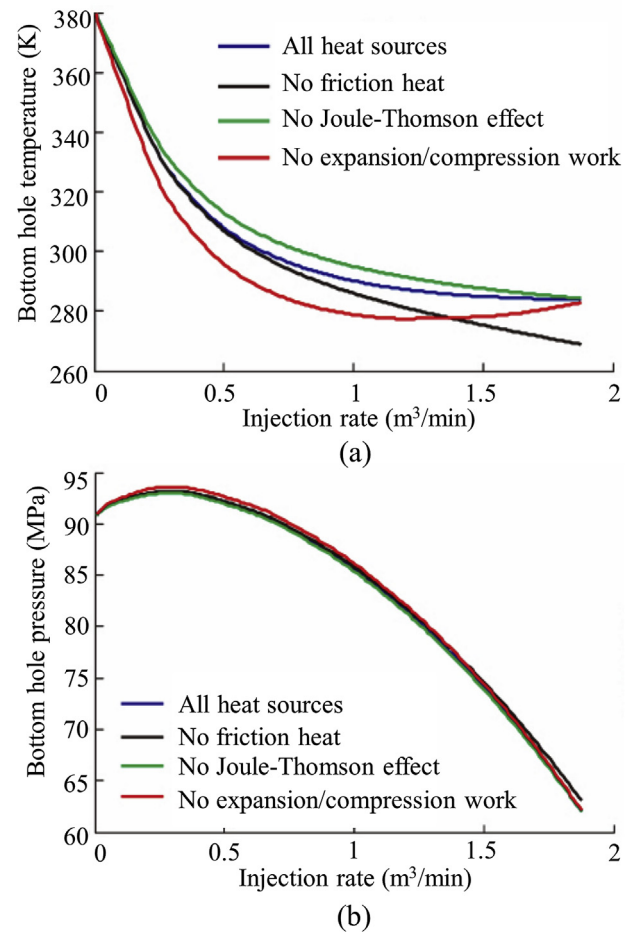


Fig. 2. Effects of heat sources on (a) BHT and (b) BHP (modified after Li et al., 2018a).

2.2. Numerical approaches to fracture initiation and propagation

SC-CO₂ has stronger compressibility and can be adsorbed by rocks, therefore the fracture initiation and propagation laws in SC-CO₂ fracturing are quite different from those of conventional hydraulic fracturing. Up to now, researchers have carried out numerous numerical simulations to figure out these laws, as shown in Table A2. It can be observed that the differences are mainly in the multi-field coupling, numerical simulation method, fracture propagation criteria, and whether fluid compressibility, rock heterogeneity, and weak planes are considered.

Zhang et al. (2017a) used the damage evolution law (DEL) to simulate the fracture initiation and propagation in SC-CO₂ fracturing, and a coupled hydraulic-mechanical (HM) model was established. After that, many models were developed with DEL (e.g. Liu et al., 2018; Zhang et al., 2018, 2019, 2021a, b; Jia et al., 2020; Xue et al., 2021). Zhang et al. (2021a) took temperature into account and then established a fully coupled thermal-hydraulic-mechanical (THM) model, as shown in Eqs. (3)–(5), in which the compressibility of SC-CO₂ was considered:

$$Gu_{i,jj} + \frac{G}{1-2\nu}u_{j,ji} - \alpha p_{,i} - K\alpha_T T_{,i} + F_i = 0 \quad (3)$$

$$-c_1 \frac{\partial \varepsilon_v}{\partial t} - c_2 \frac{\partial T}{\partial t} + c_3 \frac{\partial p}{\partial t} = \nabla \cdot \left[\frac{k}{\mu} (\nabla p + \rho_g g \nabla z) \right] \quad (4)$$

$$c_M \frac{\partial T}{\partial t} + (T_0 + T)K\alpha_T \frac{\partial \varepsilon_T}{\partial t} + \rho_g c_g (T_0 + T) \frac{k}{\mu} \nabla p = \lambda_M \nabla^2 T \quad (5)$$

where G is the shear modulus; ν is the Poisson's ratio; u_i and u_j are the components of displacement in the i and j directions, respectively; α is the Biot's coefficient; p is the pressure of CO₂ in the reservoir; K is the bulk modulus of rock; α_T is the thermal expansion coefficient of rock; T is the reservoir temperature; F_i is the component of body force in the i direction; c_1 , c_2 , c_3 are the coefficients related to porosity and bulk modulus; ε_v is the volumetric strain; t is the fracturing time; k is the rock permeability; μ is the dynamic viscosity of CO₂; ρ_g is the density of CO₂ in the reservoir; g is the gravity acceleration; c_M is the effective heat capacity; T_0 is the reference temperature under zero stress state; ε_T is the strain related to temperature; c_g is the heat capacity of CO₂ in the reservoir; and λ_M is the effective thermal conductivity coefficient.

Liu et al. (2018) considered the influences of SC-CO₂ adsorption in shale gas reservoirs on both rock deformation and fluid flow, and used the Langmuir equation to describe the adsorption process. Xue et al. (2021) further considered SC-CO₂ diffusion in the coal matrix and fractures, and suggested that SC-CO₂ was in three states: free state, adsorbed state, and remaining state. The corresponding porosity evolution equation, rock deformation equation, and fluid flow equation are shown in Eqs. (6)–(8). These two models make it possible to more accurately simulate the fracture propagation of SC-CO₂ fracturing in unconventional reservoirs:

$$\frac{\partial \varphi}{\partial t} = \frac{\alpha - \varphi}{1 + S} \left[\frac{\partial \varepsilon_v}{\partial t} + \frac{1}{K_s} \frac{\partial p}{\partial t} - \frac{\varepsilon_L P_L}{(p + P_L)^2} \frac{\partial p}{\partial t} \right] \quad (6)$$

$$Gu_{i,jj} + \frac{G}{1-2\nu}u_{j,ji} - \beta_f p_{f,i} - \beta_m p_{m,i} - K\varepsilon_{s,i} + F_i = 0 \quad (7)$$

$$\varphi \frac{\partial \rho_g}{\partial t} + \rho_g \frac{\partial \varphi}{\partial t} + \frac{\partial}{\partial t} \left(\rho_{ga} \rho_r \frac{V_L p}{p + P_L} \right) + \nabla \cdot \left(-\frac{k \rho_g}{\mu} \nabla p \right) + \rho_{ga} \rho_r \frac{dm_b}{dt} = \bar{Q}_s \quad (8)$$

where φ is the porosity; S is a parameter related to the volumetric strain and adsorption strain; K_s is the bulk modulus of rock skeleton; ε_L is the Langmuir adsorption strain; P_L is the Langmuir pressure; β_f is the effective stress coefficient of fracture; p_f is the pressure of CO₂ in the fracture; β_m is the effective stress coefficient of matrix; p_m is the pressure of CO₂ in the matrix; ε_s is the adsorption strain; ρ_{ga} is the density of CO₂ under the standard state; ρ_r is the rock density; m_b is the exchange rate of CO₂ in the fracture and the matrix; and \bar{Q}_s is the mass source.

Many researchers (e.g. Liu et al., 2020; Cai and Liu, 2021; Song et al., 2021; Yang et al., 2021) also used the cohesive zone method (CZM) to simulate fracture propagation in SC-CO₂ fracturing. Liu et al. (2020) considered both viscous force and capillary pressure between SC-CO₂ and formation fluid in the model, as shown in Eq. (9). In addition, fluid flow channels in the matrix were divided into pore elements and throat elements (Fig. 3), and the calculation methods of corresponding conductivity coefficients were also proposed. The model enabled an in-depth study of the effect of capillary forces between SC-CO₂ and formation fluids on fracture initiation and propagation at the pore scale:

$$q_{ij} = C_{ij} (P_i - P_j - P_{c,ij}) \quad (9)$$

where q_{ij} is the flow rate between different pores; C_{ij} is the conductivity coefficient of the flow channel; P_i and P_j are the pressures in pores i and j , respectively; $P_{c,ij}$ is the capillary pressure between pores i and j .

Yan et al. (2019, 2021) divided SC-CO₂ fracturing in coal seams into two stages: SC-CO₂ fracturing stage and phase change fracturing stage, and used trinitrotoluene (TNT) equivalence analysis to calculate the energy generated from phase change, as shown in Eq. (10). Then, the energy was applied to the fracture surface at the end of the first stage to calculate the fracture propagation in the second stage:

$$W_{TNT} = \frac{\eta}{Q_{TNT}} \frac{P_0 V_f}{\kappa - 1} \left[1 - \left(\frac{P_{min}}{P_0} \right)^{\frac{\kappa-1}{\kappa}} \right] \quad (10)$$

where W_{TNT} is the TNT equivalence of CO₂ phase change, Q_{TNT} is the energy generated from the explosion of 1 kg TNT, η is the energy utilization efficiency; P_0 is the pressure before CO₂ phase change; V_f is the fracture volume before CO₂ phase change; κ is the adiabatic

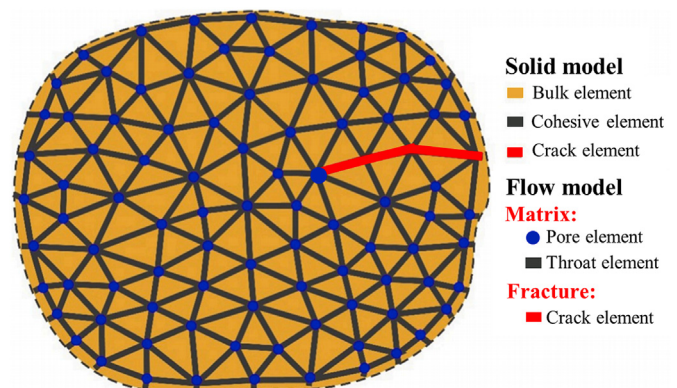


Fig. 3. Schematic diagram of flow-solid coupling model (Liu et al., 2020).

coefficient; P_{\min} is the minimum pressure required for fracture propagation.

The remaining models are deficient in considering the characteristics of SC-CO₂ fracturing fluid, so they will not be repeated here.

2.3. Numerical simulation methods for fracture propagation

2.3.1. Continuous medium methods

The continuum medium methods regard the reservoir rock as a continuum and the finite element method (FEM), boundary element method (BEM), and finite difference method (FDM) are used to solve the elastic equations.

(1) FEM-based methods

The FEM-based methods mainly include the adaptive remeshing method (ARM), extended finite element method (XFEM), cohesive zone model (CZM), phase field method (PFM), and DEL.

The ARM implies that at each time step, the mesh is dynamically updated so that the propagated fracture path matches the edge of the mesh (Funari et al., 2019). The construction of this algorithm is complicated and the computational workload is huge, and the quality of the mesh reconstruction greatly affects the accuracy of the fracture propagation simulation results.

The XFEM is a kind of FEM based on unit decomposition. It introduces the enhanced shape function of displacement discontinuity into the conventional FEM to characterize the fracture (Belytschko and Black, 1999). XFEM makes the discontinuous structures independent of the computational grid and requires no encryption of the local grid of discontinuous structures, which significantly reduces the computational workload (Bayesteh and Mohammadi, 2013). When the XFEM is applied to the fracture propagation problem, one can predict the fracture propagation in any direction without presetting the fracture propagation path (Cheng et al., 2019, 2022; Wu et al., 2019).

The CZM is based on the cohesive elements, which follows a certain constitutive model (Park and Paulino, 2015), such as the linear elastic constitutive model. When the failure criterion is met, the fracture propagates along the cohesive elements (Enayatpour et al., 2018). The CZM can be used to study the fracture propagation problem of fixed or non-fixed paths (Haddad and Sepehrnoori, 2016). The setting of cohesive elements directly affects the final fracture path. If the setting is unreasonable, the obtained fracture path will appear serrated (Lecampion et al., 2018). Gao et al. (2019a, b, c) proposed an XFEM-based CZM in response to the shortcomings of the CZM, which does not require to pre-define fracture paths and allows to simulate fracture initiation and propagation in any solution-dependent path.

The PFM introduces a scalar called fracture field into the grid of continuous media and uses the fracture field to characterize the degree of rock failure (Heider, 2021). According to the value of the fracture field on the element grid, the element can be in one of three states: no failure, partial failure, and complete failure (Ehlers and Luo, 2017). The PFM facilitates solving the conventional fracture problem in the grid. The fracture propagation model can more easily consider the effects of stress interference and rock heterogeneity. However, the fracture boundary obtained by the PFM is fuzzy, so the exact value of the fracture width cannot be directly obtained, and an equivalent fracture width can only be estimated according to the fracture field value.

The DEL implies that, with an increase in the load, as soon as stresses or strains in rock elements reach a certain level specified by the adopted damage criterion, the elements will be damaged (Tang, 1997; Zhu and Tang, 2004). The tensile failure is generally assessed

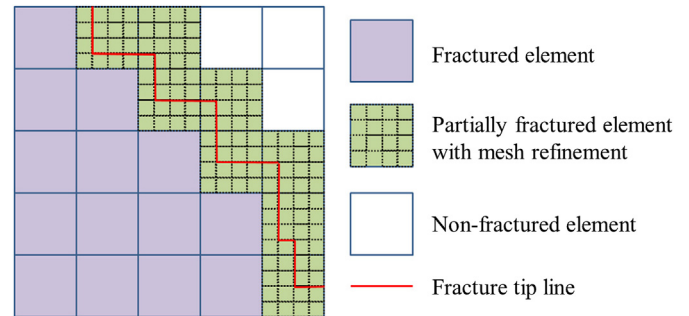


Fig. 4. Schematic diagram of mesh refinement at the fracture tip in simulating fracture propagation with FDM (Zhou et al., 2016).

via the maximum tensile stress criterion in the numerical simulation process, while the Mohr-Coulomb criterion judges the shear failure. After rock failure, its elastic modulus decreases, while the porosity and permeability increase accordingly, which can be calculated according to the damage variables and initial parameter values (Tang et al., 2002; Zhu et al., 2013). The combination of damaged elements is the fracture propagation path, and the accurate fracture width also cannot be obtained, which is identical to PFM.

The theoretical research progress of ARM, CZM, XFEM, PFM, and DEL in simulating fracture propagation can be found in the literature (e.g. Lecampion et al., 2018; Chen et al., 2021a), which will not be repeated here.

(2) BEM-based methods

As a kind of indirect BEM, the displacement discontinuity method (DDM) is mainly used to simulate fracture propagation. It was proposed by Crouch (1976) to solve the discontinuous displacement problem of isotropic media with discontinuities. Instead of discretizing the element mesh in the continuum domain by the FEM, the DDM discretizes the element mesh on the domain boundary and uses the control equation function to approximate the boundary conditions to solve the solution of the whole domain (Li et al., 2018b). Therefore, the variations of stress and displacement field in the whole rock area can be calculated by discretizing the fracture surface (Kresse and Weng, 2018). This idea of discrete boundary in the DDM provides dimension reduction. The theoretical research progress of the DDM in simulating fracture propagation can also be found in previous studies (e.g. Lecampion et al., 2018; Chen et al., 2021a).

(3) FDM-based methods

Zhou and Hou (2013) first used the FDM to simulate fracture propagation, and proposed that the fracture width was determined by the vertical stress on the fracture surface, the fluid pressure in the fracture, and the size of the fracture element, as shown in Eq. (11). The domain elements were divided into three types in this method: fractured elements, partially fractured elements, and non-fractured elements. The fracture propagation was judged by the tensile strength criterion. The filtration of fracturing fluid from the fracture to the matrix was calculated according to Darcy's law, and the flow of the matrix fluid and the deformation of the rock were calculated using the built-in model of the FLAC^{3D} software (FDM-based software). The emergence of this method provided a new idea for simulating the propagation of three-dimensional (3D) planar fractures with the FDM. Liao et al. (2019, 2020a) simulated the intersection of 3D hydraulic fractures and natural fractures with

this method. Liao et al. (2020b, c) further coupled the multiphase and multicomponent simulator TOUGH2MP to study the influence of natural fracture orientation and injection rate on heat extraction in the process of developing hot dry rock with SC-CO₂:

$$\Delta w = \frac{p_f - \sigma_3}{\alpha_1} l_c \quad (11)$$

where w is the fracture width, σ_3 is the normal stress on the fracture surface, α_1 is a parameter related to bulk modulus and shear modulus, and l_c is the element length perpendicular to the fracture propagation direction.

Zhou et al. (2014) refined the mesh of the fracture tip elements (Fig. 4), and introduced an area scale factor to improve the calculation accuracy of the fracture width and stress at the fracture tip. Moreover, the influences of proppant transport and contact stress on fracture width were considered in the model, and then the fracture propagation simulator FLAC^{3Dplus} was developed. Gou et al. (2015) further coupled FLAC^{3Dplus} and TOUGH2MP, enabling the simulation of the multiphase and multicomponent flow in fracturing. Feng et al. (2016) added thermal conduction and convection into FLAC^{3Dplus} to study the effect of temperature on fracture propagation. Zhou et al. (2016) coupled FLAC^{3Dplus} with reservoir simulator TMVOCMP to simulate multi-fracture propagation and proppant distribution in horizontal wells. Haris et al. (2020) used the FLAC^{3Dplus}-TMVOCMP simulator to explore the effects of stress shadowing on fracture propagation and heat extraction in the development of hot dry rock. Mehmood et al. (2021) further studied fracture propagation and flowback process in N-Heptane fracturing with the coupled simulator.

All aforementioned models are only suitable for simulating the propagation of 3D planar fractures. Feng (2020) divided the computational domain into multiple triangular prisms containing three splits, regarded the opening direction of the splits as the fracture propagation direction, and introduced a geometric coefficient to more accurately characterize the fracture width, as shown in Eq. (12). Then the advanced FLAC^{3Dplus} simulator was developed, which enabled the FDM to simulate the propagation of 3D fractures in arbitrary paths:

$$\Delta w = \frac{p_f - \sigma_3}{\alpha_1} l_c a_{\text{geo}} \quad (12)$$

where a_{geo} is the geometric coefficient (from 0.5 to 1).

2.3.2. Discrete medium methods

The discrete medium methods treat the entire reservoir rock as numerous solid particles or blocks from a microscopic perspective. There are two software packages based on the discrete medium methods: particle flow code (PFC) and universal distinct element code (UDEC).

(1) PFC

The PFC assumes that the microstructure of the material is statistically circular solid particles with different diameters, and the adjacent particles are given normal stiffness, shear stiffness, and friction coefficient, which transfers interaction through contact bonding and parallel bonding (Potyondy et al., 1996). The contact bonding cannot transmit torque; when the normal or tangential stress respectively exceeds the corresponding strength, the contact bonding fails (Damjanac and Cundall, 2016). The parallel bonding can transmit forces and moments; when the normal or tangential stress exceeds the corresponding strength, the parallel bonding also fails, resulting in opening or shearing microfractures,

respectively (Tomic and Gutierrez, 2017). The PFC is good at considering the interaction between rock particles or between proppants and rock particles, which is extremely helpful for understanding the microscopic mechanisms in fracturing (Kasyap et al., 2022; Luo et al., 2022b). However, the PFC only relies on circular or spherical particles, thus it cannot fully simulate the complex fracture morphology in hard rocks and mechanical behaviors such as mutual occlusion and locking between fractured blocks.

(2) UDEC

The UDEC discretizes the computational domain into a set of numerous convex polygon blocks and discontinuous structural surfaces (Zareidarmiyani et al., 2020). Inside each block, stress, strain, displacement, and other parameters are calculated. For the interaction between blocks, the tensile and shear strength criteria are followed in the normal and tangential directions, respectively (Abdollahipour et al., 2016; Rwechungula and Cheng, 2021). In the UDEC, the blocks can be fully contacted, and the random polygon blocks can be better occluded and interlocked, thus some limitations of the PFC can be overcome.

The theoretical research progress of discrete medium methods in simulating fracture propagation can be found in the literature (Lisjak and Grasselli, 2014). Since it is difficult to convert the geological parameters measured in the field into the physical parameters of spherical particles or rigid blocks, application of discrete medium methods to simulating fracture propagation is limited.

2.3.3. Comprehensive comparison

The characteristics of various numerical simulation methods for fracture propagation are listed in Table 1.

The FEM-based methods can consider reservoir heterogeneity and multi-field coupling. The computational workload is generally heavy, which are more suitable for studying the fracture propagation mechanisms in SC-CO₂ fracturing at the laboratory scale. The BEM/FDM-based methods are easy to obtain fracture parameters, and the computational workload is small, so they are more suitable for optimizing engineering parameters in SC-CO₂ fracturing at the field scale. The PFC and UDEC reflect the microscopic aspects and are more suitable for study of the micro-process.

2.4. Numerical approaches to proppant transport

SC-CO₂ fracturing fluid has a weak proppant-carrying capacity. The numerical simulations of proppant transport are helpful to figure out the proppant placement laws and further improve fracture conductivity. A lot of research work has been done to date, as shown in Table A3. It can be observed that most simulations based on computational fluid dynamics (CFD) use a small-size plane fracture as the research object without considering the dynamic propagation of the fracture. Their inlet boundary conditions imply constant volume flows and proppant volume fractions, while the outlet boundary condition involves the atmospheric pressure. The simulations based on the proppant settlement theory (PST) generally use closure stress as the outlet boundary condition and mainly consider the dynamic propagation of the fracture via the Perkins-Kern-Nordgren (PKN) model.

The CFD-based methods for simulating proppant transport can be classified into two categories: (i) the Euler-Euler method and (ii) the Euler-Lagrangian method. The first-category method, i.e. the two-fluid model, adopts the Eulerian coordinate system for the motion equations of particles and fluids. In this method, the fluid phase is treated as a continuous medium. The particle phase is

Table 1

Comprehensive comparison of numerical simulation methods for fracture propagation.

Comparison items	Continuous medium methods							Discrete medium methods	
	FEM-based					BEM-based	FDM-based	PFC	UDEC
	ARM	XFEM	CZM	PFM	DEL	DDM	FDM		
Rock heterogeneity	Y	Y	Y	Y	Y	N	Y	Y	Y
Weak planes	Y	Y	Y	Y	Y	Y	Y	Y	Y
Fracture initiation	Y	N	Y	Y	Y	N	Y	Y	Y
Multi fracture propagation	***	*	**	*	*	*	*	**	**
Multi-field coupling	*	*	*	*	*	***	*	***	***
Fracture parameter acquisition	***	*	**	**	***	*	*	***	***
Computational workload	***	**	**	**	**	*	*	***	***
Suitable scale	Lab-scale	Lab-scale	Lab-scale	Lab-scale	Lab-scale	Field-scale	Field-scale	Micro-scale	Micro-scale
Auxiliary software/code	N	ABAQUS	ABAQUS	COMSOL	COMSOL	N	FLAC ^{3D}	PFC ^{2D} /PFC ^{3D}	UDEC

Note: Y- Yes, N- No, *- Easy/Low, **- General, ***- Difficult/High.

treated as a pseudo fluid with dynamic characteristics similar to the liquid phase (McAndrew et al., 2017; Suri et al., 2020). In the Euler-Lagrangian method, the fluid is regarded as a continuous phase, while the particle phase is treated as a series of limited discrete elements. The motion of a single particle follows Newton's Second Law of motion. Its motion equation is solved in the Lagrangian coordinate system to determine the particle position and velocity at different times, reflecting the particles' motion process (Atul et al., 2013; Chen et al., 2021b). The PST-based methods generally describe the proppant particle motion through an empirical model, accounting for the fracture wall, proppant concentration, and Reynolds number effect by adopting the respective adjustment coefficients (Patankar et al., 2002; Brannon et al., 2006). Since there is no significant difference in mathematical models for simulating proppant transport in SC-CO₂ fracturing and hydraulic fracturing, the relevant mathematical models will not be repeated here. For details, please refer to the literature (Isaka et al., 2019; Zhang et al., 2021c).

The CFD-based methods are implemented using the general commercial software but have a poor adaptability to fracture propagation, and their computational workload is relatively heavy, making them more suitable for underlying mechanism-related simulations. Although the fluid-particle interaction mechanisms of PST-based methods have not been clarified yet, they can easily be coupled with fracture propagation, making them more suitable for engineering optimization.

3. Numerical findings of SC-CO₂ fracturing

Numerous findings have been obtained from numerical simulations of SC-CO₂ fracturing, which are beneficial to strengthening the understanding of the mechanisms and promoting its field implementation. Therefore, these findings are systematically reviewed in this section.

3.1. Laws of wellbore flow and heat transfer

3.1.1. Temperature-pressure variation laws

CO₂ is sensitive to temperature and pressure, making the wellbore flow and heat transfer processes very complex. Generally, the temperature of CO₂ at a fixed point in the wellbore decreases with time; with the increased depth, the temperature gradually increases with decreasing gradient (Song et al., 2017). However, there are diverse patterns on the variation of wellbore pressure in the relevant literature. Thus, Lv et al. (2015) reported that the wellbore pressure grew first and then dropped with depth, while Bai et al. (2019) claimed that the wellbore pressure increased gradually with depth. Alternatively, Yang et al. (2018a) reported that the

wellbore pressure in SC-CO₂ fracturing gradually decreased with depth due to the high wellbore friction. The reason for the diverse patterns is that the pressure differences between friction and gravity caused by engineering and formation parameters are different. In addition, it should be noted that the wellhead was injected with a constant injection rate and pressure in most simulations. Consequently, injection parameters significantly affected BHP rather than wellhead pressure, which was not consistent with the actual site condition. Wu et al. (2021) assumed a constant injection rate at the wellhead and constant pressure at the well bottom, and obtained more accurate simulation results.

The tubing and casing co-injection fracturing technology is often adopted to reduce the wellbore friction in SC-CO₂ fracturing. Gong et al. (2019a) and Wu et al. (2021) reported that due to the large flow cross-sectional area of co-injection and relatively small flow velocity in the wellbore, it exhibited higher BHT and longer unsteady period, as shown in Fig. 5. It can be observed that co-injection has a lower wellhead pressure than tubing injection. Moreover, when the tubing and annulus were injected according to the proportion of their cross-sectional areas, both had lower wellhead pressure (Wu et al., 2021).

The SC-CO₂ coiled tubing jet fracturing technology can be used on site to improve the stimulation effect or realize fixed-point fracturing (Song et al., 2017). This technology also adopts coiled tubing and annulus co-injection, and a nozzle is installed at the bottom of the coiled tubing. Hence, the temperature in the tubing first gradually increases with depth, and then drops sharply after CO₂ flows through the nozzle due to the strong throttling effect of the nozzle (Yang et al., 2018b; Yi et al., 2019). There is also a large flow channel for CO₂, so the pressure in the wellbore generally increases with depth, and the pressure in the coiled tubing generally exceeds that in the annulus (Cheng et al., 2014).

3.1.2. Phase state control methods

In fracturing, the possible variation of the CO₂ phase state is depicted in Fig. 6. It can be observed that BHP generally exceeds CO₂ critical pressure, while BHT may not reach the critical temperature. In order to control CO₂ to reach the supercritical state at the well bottom, one should ensure that its temperature reaches the critical level (Cheng et al., 2014; Wang et al., 2018a). In SC-CO₂ fracturing, engineering parameters (e.g. injection temperature, injection rate, injection pressure, and well structure) and formation parameters (e.g. geothermal gradient and reservoir lithology) have certain impacts on BHT. It is vital to figure out the impacts of these parameters for better guiding the controlling of phase state.

Generally speaking, the higher the wellhead injection temperature, the greater the geothermal gradient, the larger the cross-sectional area of the flow channel, and the higher BHT (Wang

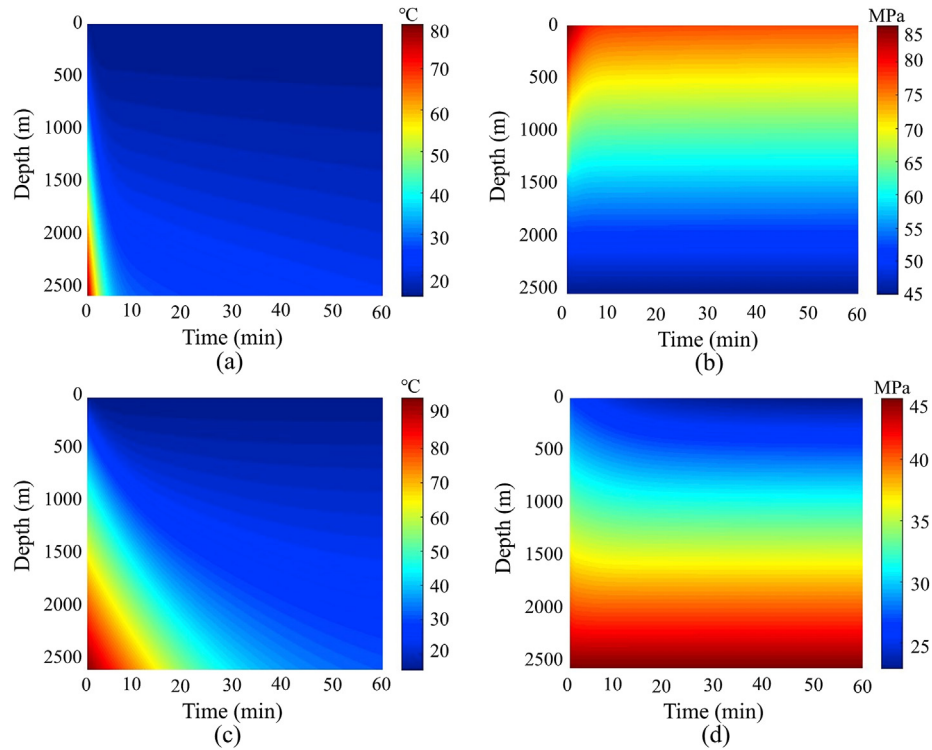


Fig. 5. Evolutions of temperature and pressure in the tubing: (a) Temperature with tubing injection; (b) Pressure with tubing injection; (c) Temperature with co-injection; and (d) Pressure with co-injection (modified after Wu et al., 2021).

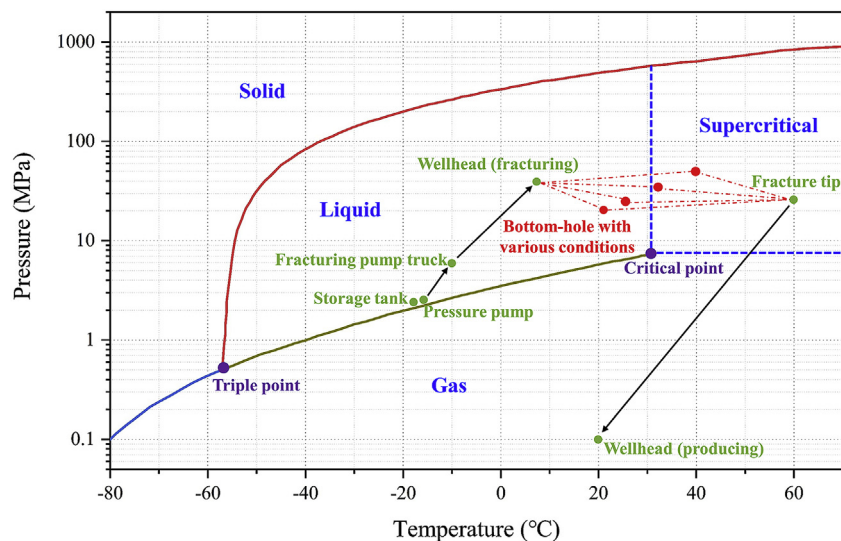


Fig. 6. The variation of CO₂ phase state in fracturing (modified after Lyu et al., 2018a).

et al., 2018a; Gong et al., 2019b). The injection rate effect on BHT is much more complicated. When the injection rate is small in a vertical well, BHT decreases gradually with the injection rate. When the injection rate exceeds a certain critical value, the friction heat generated from the increased injection rate may gradually increase the BHT (Lyu et al., 2018b), as shown in Fig. 7. In horizontal wells, due to the existence of the horizontal part, BHT grows at low injection rates and drops at medium ones (Lyu et al., 2021). The injection pressure and reservoir lithology have a minor impact on BHT (Dou et al., 2013; Guo et al., 2015).

Therefore, when the reservoir depth or geothermal gradient is small, the following procedures can be adopted to ensure that CO₂ reaches the well bottom in the supercritical state: (i) increasing the injection rate in vertical wells or reducing the injection rate in horizontal wells, (ii) using large-diameter tubing injection, tubing and annulus co-injection, or casing injection, and (iii) increasing the injection temperature at the wellhead. However, the higher injection rate in the vertical wells and the larger wellbore friction will increase the fracturing safety risk. The injection rate in horizontal wells is too low, which is not conducive to fracture

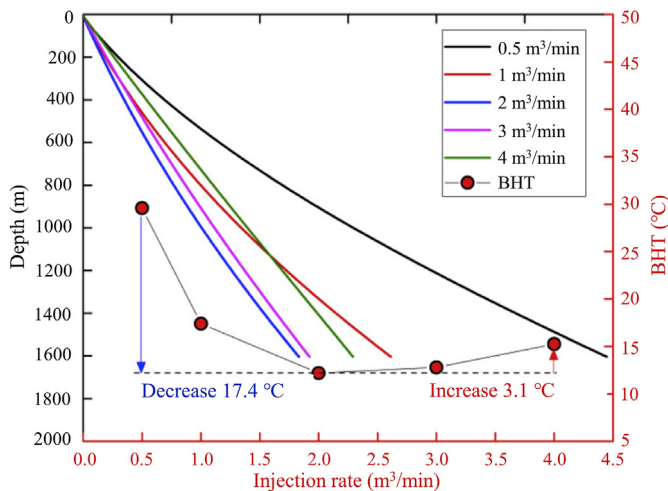


Fig. 7. Injection rate effect on BHT (Lyu et al., 2018b).

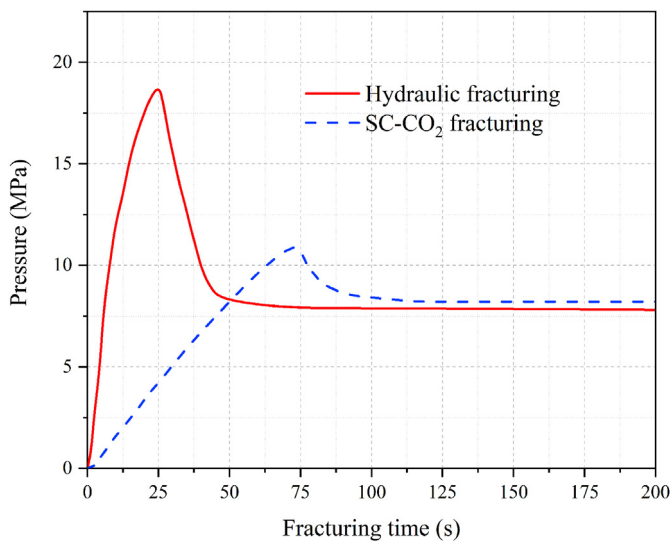


Fig. 8. Pressure evolutions in SC-CO₂ fracturing and hydraulic fracturing (modified after Yang et al., 2021).

propagation and proppant carrying, and it is easy to cause sand plugging. In addition, the large-diameter tubing is not conducive to later production, the co-injection or casing injection will damage the casing, and there is no time for adjustment in case of sand plugging. Hence, the most efficient and safest method is to place a heating device at the wellhead to increase the injection temperature of CO₂.

3.2. Laws of fracture initiation and propagation

3.2.1. Fracture initiation laws

SC-CO₂ fracturing fluid has lower viscosity and easier filtration than water-based fracturing fluid (Wang et al., 2017; Luo et al., 2021a). Filtration before fracture initiation leads to greater pore pressure increment and induced stress, thus, SC-CO₂ fracturing has a lower initiation pressure than hydraulic fracturing (Ha et al., 2018; Li et al., 2019a). However, the rapid pressure propagation caused by fracturing fluid filtration requires longer pressure holding time and more intensive fracturing fluid injection before fracture initiation (Ha et al., 2018; Yang et al., 2021), as shown in Fig. 8. Moreover, the

fracture initiation pressure of SC-CO₂ fracturing is lower than that of liquid CO₂ fracturing (Li and Zhang, 2019) and higher than that of nitrogen fracturing (Zhang et al., 2017a).

The smaller the reservoir permeability, the greater the Biot's coefficient; the smaller the confining pressure, the smaller the stress difference; the smaller the pore pressure, and the greater the fracture initiation pressure (Zhang et al., 2017a; Liu et al., 2018; Li and Zhang, 2019). The adsorption of SC-CO₂ in unconventional reservoirs also greatly impacts fracture initiation pressure (Xue et al., 2021). In addition, the smaller the injection rate (Li and Zhang, 2019), the higher the temperature of injected CO₂ (Zhang et al., 2018), and the smaller the viscosity of SC-CO₂ fracturing fluid (Liu et al., 2018), the smaller the fracture initiation pressure. Therefore, when the fracture initiation pressure is too high in SC-CO₂ fracturing, it can be reduced by adjusting the injection parameters such as injection rate and injection temperature.

3.2.2. Fracture propagation laws

SC-CO₂ fracturing fluid can be miscible with reservoir hydrocarbons, resulting in low capillary forces (Liu et al., 2020), and the seepage effect can be enhanced. Therefore, the pore pressure can grow more, increasing the probability of shear failure and mixing failure (Cai and Liu, 2021), and forming a complex fracture network (Peng et al., 2017). Jia et al. (2020) defined the fracture tortuosity by the ratio of the flow channel length to the linear length at both ends to represent the fracture complexity, and reported that SC-CO₂ fracturing had higher fracture tortuosity than liquid CO₂ fracturing, hydraulic fracturing, and viscous oil fracturing, but smaller than nitrogen fracturing, as shown in Fig. 9. The reason is that viscous oil has the highest viscosity, while nitrogen has the lowest viscosity. After the fracture propagation, energy re-concentration is required, so the fracture continuity and smoothness are poor in SC-CO₂ fracturing (Li et al., 2019a).

The fracture propagation laws of SC-CO₂ fracturing are more complicated in unconventional reservoirs due to the adsorption of SC-CO₂ on the rock surface and the existence of weak planes, such as natural fractures and bedding planes (BPs). Artificial fractures in SC-CO₂ fracturing can penetrate natural fractures and propagate in the matrix (Song et al., 2019). Besides, they can also merge with natural fractures (Fang et al., 2014; Zhao et al., 2021), thus easily forming a larger stimulated reservoir volume (SRV). In the case of BPs, three modes of intersection (propagating along BPs, penetrating BPs, and offset BPs) between the artificial fractures and BPs were revealed by Luo et al. (2021b). Alternatively, Zhang et al. (2021b) revealed the following four modes: inserting, L-type, T-type, and direct crossing, as shown in Fig. 10. The smaller the dip angle and the greater the stiffness of BPs, the easier it is to develop the intersection mode from other modes to direct crossing. Among the three types of BPs (horizontal BPs, vertical BPs, and orthogonal BPs), the first two types restrict the fracture propagation in the other direction (Zhang et al., 2019), so reservoirs with orthogonal BPs are more likely to form a complex fracture network (Luo et al., 2021b). In addition, the expansion stress induced by SC-CO₂ adsorption on coalbed and shale can increase the chance of rock damage and facilitate the formation of a complex fracture network (Zhang et al., 2017b; Liu et al., 2018). In the case of shallow coalbed, Yan et al. (2019, 2020, 2021) revealed that the phase changed fracturing stage after the SC-CO₂ fracturing stage, and the fracture propagation mainly occurred in the first stage, accounting for 80%–90% of the fracture length, while the contribution to the fracture width was nearly the same in the two stages.

In addition, geological and engineering parameters also have different impacts. For example, the higher the reservoir temperature, the higher the elastic modulus (He et al., 2020), and the longer and narrower the fracture (Song et al., 2021). With the horizontal

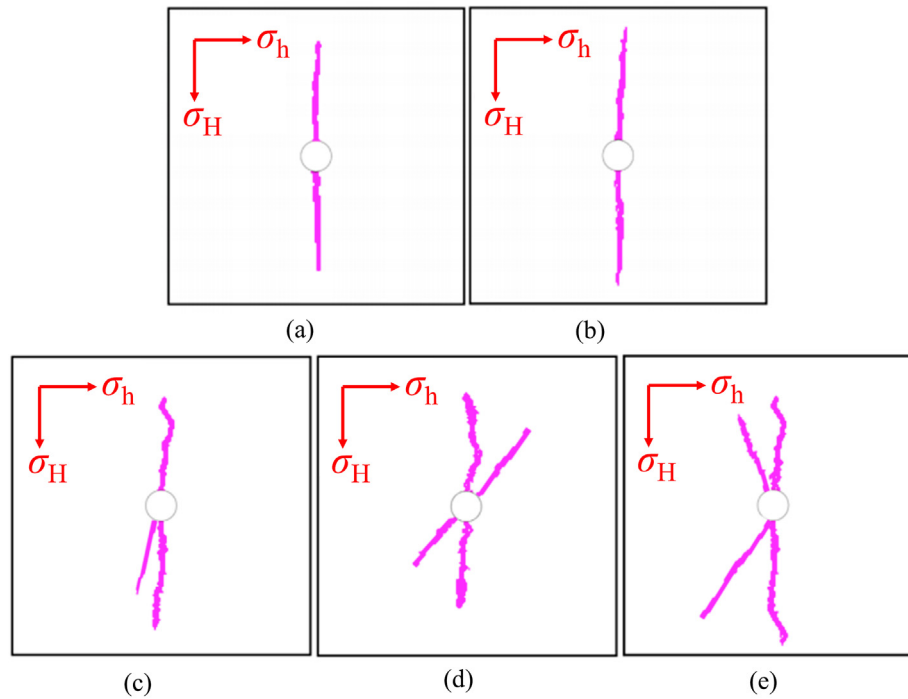


Fig. 9. Fracture morphology with different fracturing fluids: (a) Viscous oil; (b) Water; (c) L-CO₂; (d) SC-CO₂; and (e) Nitrogen (Jia et al., 2020).

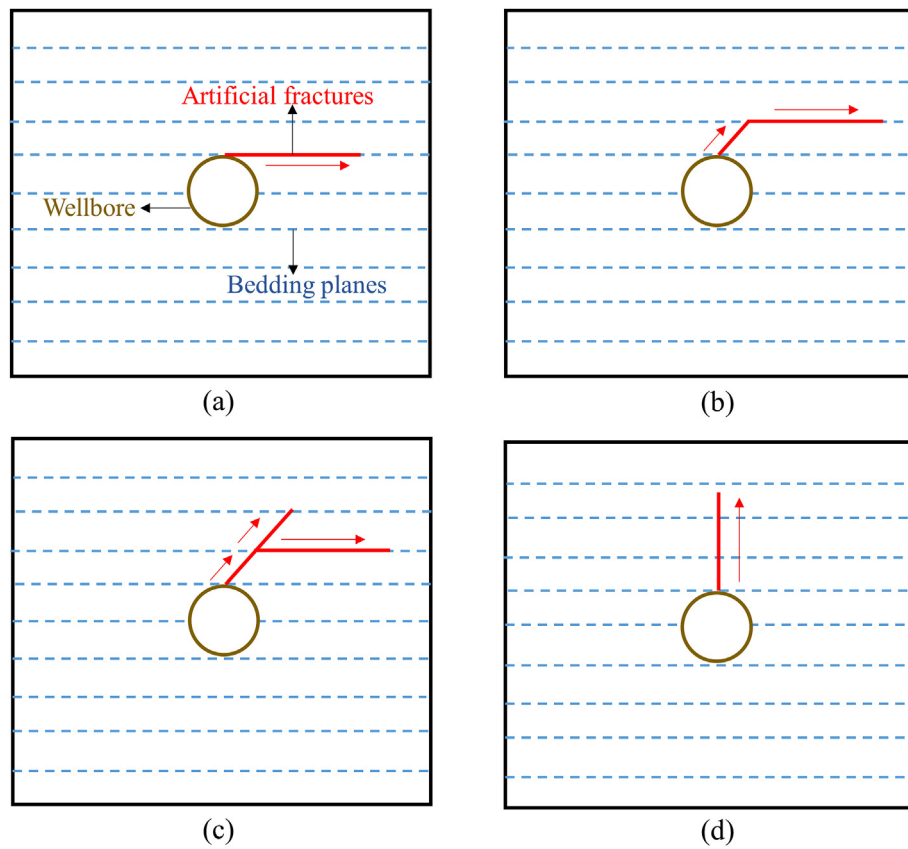


Fig. 10. Four intersection modes of artificial fractures and bedding planes in SC-CO₂ fracturing: (a) Inserting; (b) L-type; (c) T-type; and (d) Crossing (modified after Zhang et al., 2021b).

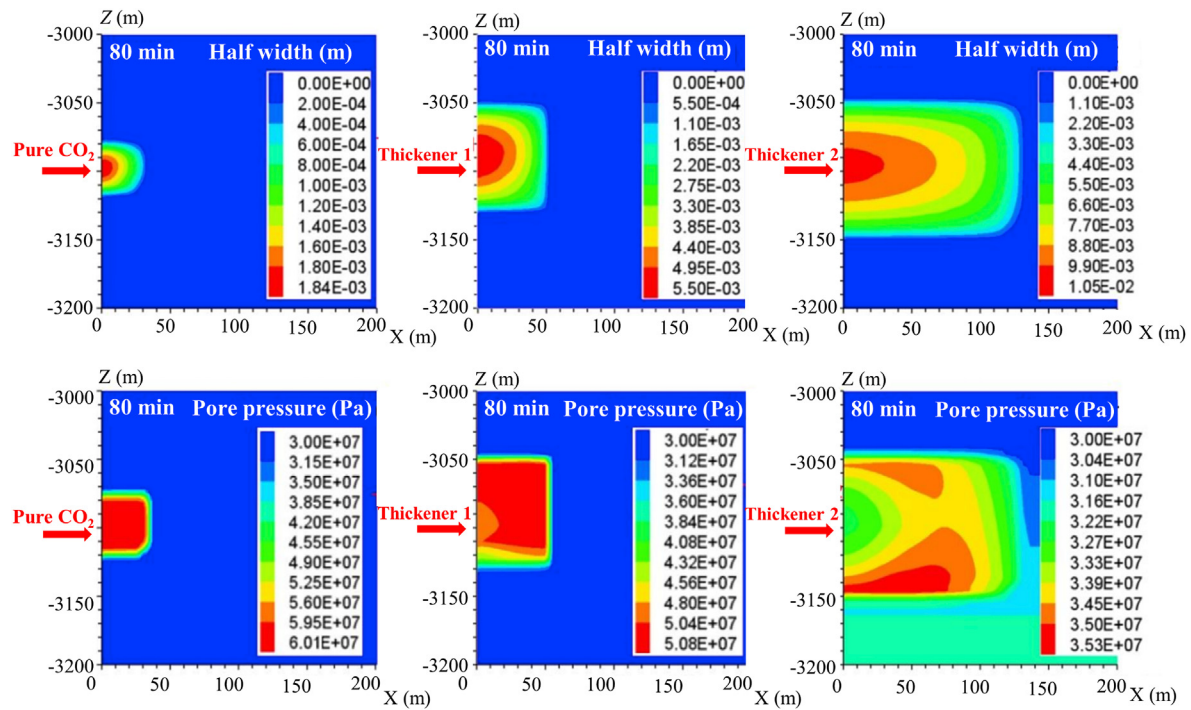


Fig. 11. Fracture width and pore pressure before and after SC- CO_2 thickening (modified after Liao, 2020).

stress difference increasing, the fracture morphology will change from a complex fracture network to a single fracture, but SC- CO_2 fracturing has a strong ability to resist this change (Guo et al., 2022). The greater the reservoir permeability, the shorter and narrower the fracture. When the reservoir permeability is high, the more the filtration of SC- CO_2 fracturing fluid and the faster the energy dissipation, inhibiting further fracture propagation (Guo et al., 2022). Therefore, it is necessary to add a thickener into the fracturing fluid to reduce the filtration (Li et al., 2019b). The fracture width and pore pressure before and after SC- CO_2 thickening are shown in Fig. 11. Still, the increase of SC- CO_2 viscosity after thickening will reduce the fracture network complexity. Furthermore, the larger the injection rate, the higher the possibility of forming a complex fracture network (Zhang et al., 2021a), and the greater the fracture width. Therefore, the problem of difficult proppant transports caused by insufficient fracture width can be mitigated by increasing the injection rate (He et al., 2020). Meanwhile, the wellbore friction also inevitably increases.

The technology of SC- CO_2 fracturing followed by thickened SC- CO_2 fracturing (Li and Zhang, 2019) can be adopted to increase the width of fractures while forming a complex fracture network. It is also practicable to increase the injection rate (Li et al., 2019b) on the premise of adding a high-efficiency drag reducer into the fracturing fluid. Still, the injection rate should not be too high so as to avoid affecting the integrity of the cement sheath, otherwise, it is not conducive to later production and CO_2 sequestration (Genedy et al., 2014, 2017; Stormont et al., 2018).

3.3. Laws of proppant transport

The proppant placement in the fracture can be subdivided into three stages in SC- CO_2 fracturing. At the first stage (flat laying), the proppant settles near the jet stagnation point due to gravity, forming a proppant dune at the fracture bottom. At the second stage (proppant dune development), the proppant dune height grows continuously with the settlement of proppant particles,

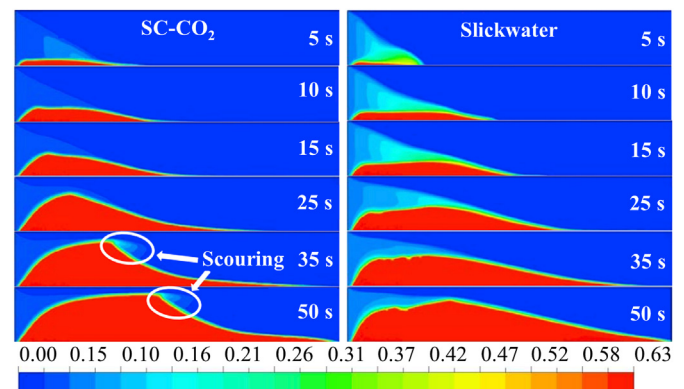


Fig. 12. The proppant distribution in SC- CO_2 fracturing and slickwater fracturing (modified after Zheng et al., 2020b).

forming a bulge at a certain position from the inlet. Finally, after the proppant dune reaches the equilibrium height, the proppant bank continues to extend towards the outlet, corresponding to the proppant bank development stage (Wang et al., 2018b; Zheng et al., 2020a). The proppant distribution characteristics in SC- CO_2 fracturing fluid are similar to those in the slickwater fracturing fluid. There are four areas according to the proppant concentration: the low-land area, the suspension area, the tumbling area, and the proppant bank area (Xiao et al., 2018). The proppant bank area and the suspension area are the two key regions controlling the fracture shape (Song et al., 2018). However, the proppant-carrying capacity of SC- CO_2 is weaker than that of slickwater (Zheng et al., 2020b), as shown in Fig. 12. As a result, SC- CO_2 fracturing can form higher proppant banks (Song et al., 2018) or may cause sand plugging in a shorter time (Wang and Elsworth, 2020).

When non-smooth or no-plane fractures are formed in SC- CO_2 fracturing, the proppant transport laws become more complex. If

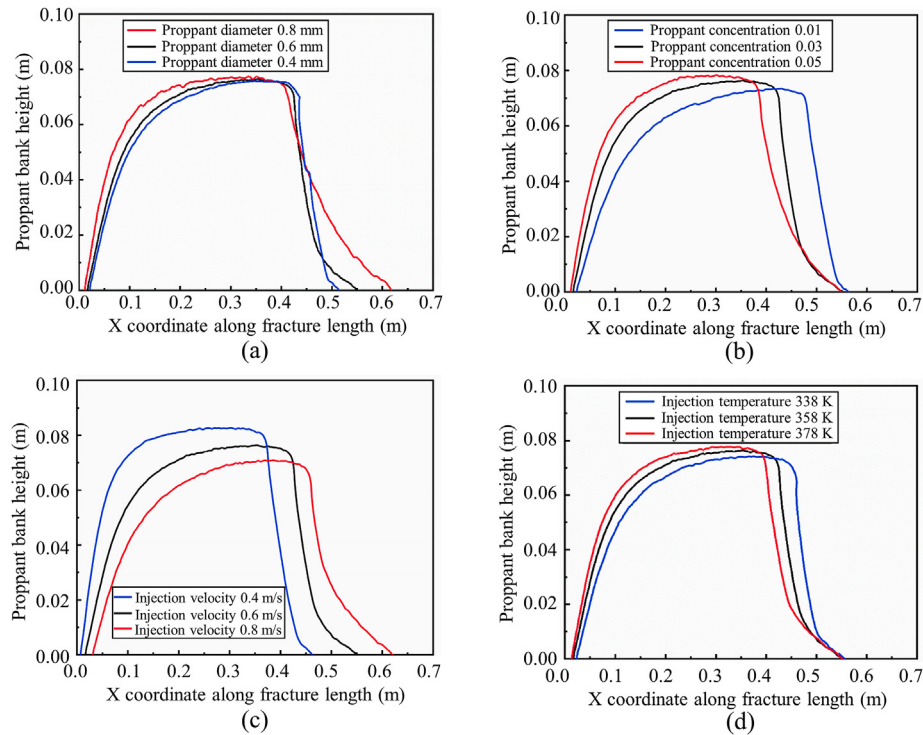


Fig. 13. Effects of (a) Proppant diameter; (b) Proppant concentration; (c) Injection velocity; and (d) Injection temperature on the proppant bank (modified after Zheng et al., 2020a).

complex fractures are formed by fracturing, there are two main ways for proppant to flow into branch fractures. The first one envisages that after the early proppant has formed a proppant bank at the root of the branch fractures, the subsequent proppant rolls into the branch fractures by gravity. The second way implies that proppant is carried into the branch fractures by the flow of SC-CO₂ fracturing fluid (Ge et al., 2019). If the fracture is T-shaped, the strong turbulence can bring proppant into the branch fractures. If the fracture shape is a crossing junction, most proppant is left in the main fracture, while its small share enters the branch fractures. The larger the cross angle, the harder for the proppant to enter the branch fractures (Wang et al., 2018c). If the curved fracture with an uneven surface is formed, the proppant will not form a proppant bank but accumulate in a narrow zone (Xu et al., 2020).

Proppant properties, fracturing fluid properties, and injection parameters also control the proppant transport and placement in fractures, as shown in Fig. 13. Although the equilibrium height of the proppant bank decreases slightly (Zhou et al., 2020), lower proppant density and particle size, higher viscosity of SC-CO₂ fracturing fluid increase the proppant placement length along the fracture propagation direction (Sun et al., 2018). Thus, longer and lower propped fractures can be obtained (Song et al., 2018). Increasing the injection rate is conducive to improving the proppant-carrying effect of SC-CO₂ fracturing fluid (Wang et al., 2019b). At high injection rates and Reynolds numbers, SC-CO₂ and slickwater fracturing fluids have nearly identical proppant-carrying performances (Hou et al., 2017; Sun et al., 2018). The temperature of injected CO₂ has an ambiguous effect on the proppant transport: the increased injection temperature reduces the viscosity and density of SC-CO₂ fracturing fluid, hindering the proppant transport (Zheng et al., 2020b, 2021), but also increases the fracturing fluid velocity, with the opposite effect (Zheng et al., 2020b). As a result, the temperature effect needs to be

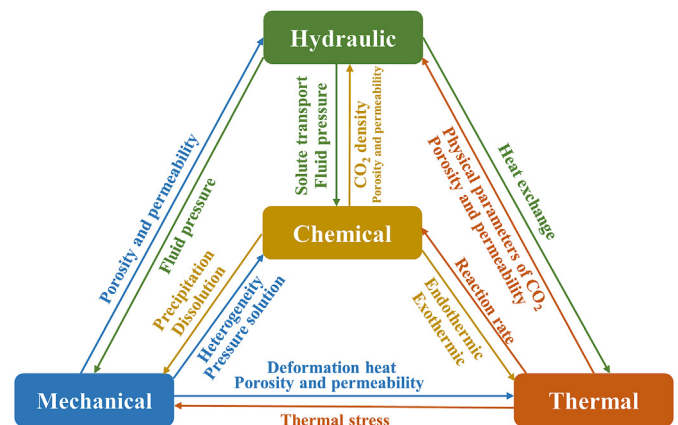


Fig. 14. THMC coupling processes in SC-CO₂ fracturing.

comprehensively analyzed for particular geological and engineering parameters.

In addition, the way and location of proppants entering the fracture also impact the placement of proppants. Compared with the cuboid inlet, the nozzle inlet can form a homogeneous proppant bank in the near-wellbore area of the fracture (Zhou et al., 2020). The higher the height of the injection point, the greater the turbulence degree near the wellbore. As a result, proppants are more evenly distributed near the wellbore (Zheng et al., 2021), thus forming a higher conductivity in the well vicinity.

In order to improve the proppant placement effect in SC-CO₂ fracturing, light-weight and small-sized proppant particles and thickened SC-CO₂ fracturing fluid can be adopted in conjunction with the increased injection rate and centralized perforation in the upper part of the reservoir.

4. Limitations of previous numerical simulations and possible mitigation

Although previous numerical simulations of SC-CO₂ fracturing have revealed numerous findings, there are still some limitations:

- (1) Despite a large number of proposed wellbore flow and heat transfer models for different SC-CO₂ fracturing technologies in vertical wells, most of them ignore the effects of CO₂ phase change and proppant on temperature and pressure. Moreover, these models envisage that the well bottom is open, while before the fracture initiation, its cross-section is limited, and the CO₂ in the wellbore is continuously compressed. Therefore, the effect of CO₂ phase change and the actual fracturing processes (such as proppant transport and pressure holding in the wellbore before fracture initiation) should also be considered in the refined models, so as to improve the prediction accuracy of the CO₂ phase state in both vertical and horizontal wells.
- (2) The previous numerical simulations of fracture propagation mainly focus on HM or THM couplings, ignoring the chemical field-related interactions. These simulations are mainly two-dimensional lab-scale ones, which are hardly adaptable to the field operative conditions. Moreover, the main findings on the initiation and propagation of SC-CO₂ fracturing concern the surface phenomena, while the respective mechanisms in the deep core remain unclear. Therefore, it is necessary to adopt appropriate numerical simulation methods to establish the 3D non-planar model of fracture initiation and propagation for SC-CO₂ fracturing with thermal-hydraulic-mechanical-chemical (THMC) coupling (Fig. 14), and deeply explore the initiation and propagation mechanisms of complex fractures at the field scale.
- (3) The previous numerical simulations of proppant transport mainly focus on small-size plane fractures and rarely consider the dynamic propagation of fractures. A few attempts to do this mainly involve the PKN model, failing to account for the complex fracture network formed by the SC-CO₂ fracturing. Therefore, it is necessary to further consider the compression or expansion, phase change and other characteristics of SC-CO₂ fracturing fluid, and couple the proppant transport with the dynamic propagation of complex fractures, so as to better optimize the injection parameters and improve the proppant placement effect.

5. Conclusions

This paper systematically reviews the numerical simulations of wellbore flow and heat transfer, fracture initiation and propagation, and proppant transport in SC-CO₂ fracturing. The main conclusions are as follows:

- (1) The variations of wellbore temperature and pressure are complex and strongly transient in SC-CO₂ fracturing. When the wellbore friction is large, the wellhead pressure can be reduced by tubing and annulus co-injection or adding a drag reducer. When the reservoir depth is shallow, or the geothermal gradient is small, the temperature of CO₂ can be increased by wellhead heating to promote CO₂ reaching the supercritical state at the well bottom.
- (2) The low viscosity and easy filtration of SC-CO₂ fracturing fluid reduce the fracture initiation pressure and increase fracture complexity, but the fracture width remains relatively narrow. The technology of SC-CO₂ fracturing followed

by thickened SC-CO₂ fracturing, combining with high injection rates, can form a complex fracture network and ensure the required fracture width.

- (3) SC-CO₂ fracturing fluid has a weak proppant-carrying capacity, which may cause sand plugging. Light and small-sized proppant particles and thickened SC-CO₂ fracturing fluid can be adopted in conjunction with the increased injection rate and centralized perforation in the upper part of the reservoir so as to improve the proppant placement effect.
- (4) The interactions between wellbore flow and heat transfer, fracture initiation and propagation, and proppant transport are complex in SC-CO₂ fracturing, and the mechanisms are not clear. Follow-up research is required to get a deeper insight into the SC-CO₂ fracturing mechanisms. Finally, more cost-effective drag reducers, thickeners, and ultra-light proppants suitable for SC-CO₂ fracturing should be developed to further promote the steady development and field application of SC-CO₂ fracturing technology.

Declaration of competing interest

The authors declare that they have no known competing financial interests or personal relationships that could have appeared to influence the work reported in this paper.

Acknowledgments

This work is funded by the Henan Institute for Chinese Development Strategy of Engineering & Technology (Grant No. 2022HENZDA02) and the China Scholarship Council (No. 202208080058). Our great thanks give to the handling editor and anonymous reviewers for their detailed and constructive reviews.

Appendix A. Supplementary data

Supplementary data to this article can be found online at <https://doi.org/10.1016/j.jrmge.2022.08.008>.

References

- Abdollahipour, A., Marji, M.F., Bafghi, A.Y., Gholamnejad, J., 2016. DEM simulation of confining pressure effects on crack opening displacement in hydraulic fracturing. *Int. J. Min. Sci. Technol.* 26 (4), 557–561.
- Ali, M., Shar, A.M., Mahesar, A.A., et al., 2022. Experimental evaluation of liquid nitrogen fracturing on the development of tight gas carbonate rocks in the Lower Indus Basin, Pakistan. *Fuel* 309, 122192.
- Atul, B., Siddharth, J., Yogesh, D., Freddy, C., 2013. Transport and distribution of proppant in multistage fractured horizontal wells: a CFD simulation approach. In: *SPE Annual Technical Conference and Exhibition*. OnePetro, New Orleans, Louisiana, USA, SPE-166096-MS.
- Bai, J.W., Xiao, C.Y., Mu, C.G., Zheng, L.H., 2019. Study on the wellbore flow for carbon dioxide fracturing. *Appl. Sci.* 9 (9), 1864.
- Barbati, A.C., Desroches, J., Robisson, A., McKinley, G.H., 2016. Complex fluids and hydraulic fracturing. *Annu. Rev. Cell Biol.* 7, 415–453.
- Bayesteh, H., Mohammadi, S., 2013. XFEM fracture analysis of orthotropic functionally graded materials. *Compos. B Eng.* 44 (1), 8–25.
- Belytschko, T., Black, T., 1999. Elastic crack growth in finite elements with minimal remeshing. *Int. J. Numer. Methods Eng.* 45 (5), 601–620.
- Bennour, Z., Ishida, T., Nagaya, Y., et al., 2015. Crack extension in hydraulic fracturing of shale cores using viscous oil, water, and liquid carbon dioxide. *Rock Mech. Rock Eng.* 48 (4), 1463–1473.
- Brannon, H.D., Wood, W.D., Wheeler, R.S., 2006. Improved understanding of proppant transport yields new insight to the design and placement of fracturing treatments. In: *SPE Annual Technical Conference and Exhibition*. OnePetro, San Antonio, Texas, USA, SPE-102758-MS.
- Brown, D.W., 2000. A hot dry rock geothermal energy concept utilizing supercritical CO₂ instead of water. In: *Proceedings of the Twenty-Fifth Workshop on Geothermal Reservoir Engineering*. Stanford University, Stanford, California, USA, pp. 233–238.
- Cai, X., Liu, W., 2021. Hydromechanical-coupled cohesive interface simulation of complex fracture network induced by hydrofracturing with low-viscosity supercritical CO₂. *Lithosphere* 2021 (Special 1), 6689981.

- Cao, C., Hou, Z.M., Li, Z.Y., Pu, X.L., Liao, J.X., Wang, G., 2022. Numerical modeling for CO₂ storage with impurities associated with enhanced gas recovery in depleted gas reservoirs. *J. Nat. Gas Sci. Eng.* 102, 104554.
- Chen, N.H., 1979. An explicit equation for friction factor in pipe. *Ind. Eng. Chem. Fundam.* 18 (3), 296–297.
- Chen, H., Hu, Y., Kang, Y., Cai, C., Liu, J.W., Liu, Y.W., 2019. Fracture initiation and propagation under different perforation orientation angles in supercritical CO₂ fracturing. *J. Petrol. Sci. Eng.* 183, 106403.
- Chen, B., Barboza, B.R., Sun, Y.N., et al., 2021a. A review of hydraulic fracturing simulation. *Arch. Comput. Methods Eng.* 29, 1–58.
- Chen, M., Guo, T.K., Zou, Y.S., Zhang, S.C., Qu, Z.Q., 2021b. Numerical simulation of proppant transport coupled with multi-planar-3D hydraulic fracture propagation for multi-clusterfracturing. *Rock Mech. Rock Eng.* 55 (2), 565–590.
- Cheng, Y.X., Li, G.S., Wang, H.Z., Shen, Z.H., Cai, C.Z., 2014. Phase control of wellbore fluid during supercritical CO₂ jet fracturing. *Acta Pet. Sin.* 35 (6), 1182–1187 (in Chinese).
- Cheng, L., Luo, Z.F., Yu, Y., Zhao, L.Q., Zhou, C.L., 2019. Study on the interaction mechanism between hydraulic fracture and natural karst cave with the extended finite element method. *Eng. Fract. Mech.* 222, 106680.
- Cheng, L., Luo, Z.F., Zhao, L.Q., Xie, Y.Z., 2022. Numerical analysis of fracture deformation and instability during CO₂ geological sequestration using a THM-XFEM coupled model. *Comput. Geotech.* 145, 104664.
- Crouch, S.L., 1976. Solution of plane elasticity problems by the displacement discontinuity method. I. Infinite body solution. *Int. J. Numer. Methods Eng.* 10 (2), 301–343.
- Damjanac, B., Cundall, P., 2016. Application of distinct element methods to simulation of hydraulic fracturing in naturally fractured reservoirs. *Comput. Geotech.* 71, 283–294.
- Dou, L.B., Li, G.S., Shen, Z.H., Wu, C.F., Bi, G., 2013. Wellbore pressure and temperature prediction model and its affecting factors for CO₂ injection wells. *Pet. Drill. Tech.* 41 (1), 76–81 (in Chinese).
- Ehlers, W., Luo, C.Y., 2017. A phase-field approach embedded in the theory of porous media for the description of dynamic hydraulic fracturing. *Comput. Methods Appl. Math.* 315, 348–368.
- Enayatpour, S., Oort, V.E., Patzek, T., 2018. Thermal shale fracturing simulation using the cohesive zone method (CZM). *J. Nat. Gas Sci. Eng.* 55, 476–494.
- Estrada, J.M., Bhamidimarri, R., 2016. A review of the issues and treatment options for wastewater from shale gas extraction by hydraulic fracturing. *Fuel* 182, 292–303.
- Fang, C., Chen, W., Amro, M., 2014. Simulation study of hydraulic fracturing using super critical CO₂ in shale. In: Abu Dhabi International Petroleum Exhibition and Conference. OnePetro, Abu Dhabi, UAE. SPE-172110-MS.
- Feng, W.T., Were, P., Li, M.T., Hou, Z.M., Zhou, L., 2016. Numerical study on hydraulic fracturing in tight gas formation in consideration of thermal effects and THM coupled processes. *J. Petrol. Sci. Eng.* 146, 241–254.
- Feng, W.T., 2020. Numerical Study of the Stimulation Related Thermo-Hydro-Mechanical Processes in Tight Gas and Deep Geothermal Reservoirs, first ed. Cuvillier Verlag, Göttingen, Germany.
- Fenghour, A., Wakeham, W.A., Vesovic, V., 1998. The viscosity of carbon dioxide. *J. Phys. Chem. Ref. Data* 27 (1), 31–44.
- Funari, M.F., Lonetti, P., Spadea, S., 2019. A crack growth strategy based on moving mesh method and fracture mechanics. *Theor. Appl. Fract. Mech.* 102, 103–115.
- Gale, J.F., Laubach, S.E., Olson, J.E., Eichhubl, P., Fall, A., 2014. Natural fractures in shale: a review and new observations. *AAPG Bull.* 98 (11), 2165–2216.
- Gao, Q., Cheng, Y.F., Han, S.C., Yan, C.L., Jiang, L., 2019a. Numerical modeling of hydraulic fracture propagation behaviors influenced by pre-existing injection and production wells. *J. Petrol. Sci. Eng.* 172, 976–987.
- Gao, Q., Cheng, Y.F., Han, S.C., et al., 2019b. Exploration of non-planar hydraulic fracture propagation behaviors influenced by pre-existing fractured and unfractured wells. *Eng. Fract. Mech.* 215, 83–98.
- Gao, Q., Han, S.C., Cheng, Y.F., Yan, C.L., Sun, Y.W., Han, Z.Y., 2019c. Effects of non-uniform pore pressure field on hydraulic fracture propagation behaviors. *Eng. Fract. Mech.* 221, 106682.
- Ge, Q., Ma, X.F., Zhang, S.C., Cao, T., Li, S.H., 2019. Numerical simulation of proppant carrying law of CO₂ fluid in complex fractures. *J. Xi'an Shiyou Univ. Nat. Sci. Ed.* 34 (3), 41–48 (in Chinese).
- Genedy, M., Stormont, J., Matteo, E., Taha, M.R., 2014. Examining epoxy-based nanocomposites in wellbore seal repair for effective CO₂ sequestration. *Energy Proc.* 63, 5798–5807.
- Genedy, M., Kandil, U.F., Matteo, E.N., Stormont, J., Taha, M.M.R., 2017. A new polymer nanocomposite repair material for restoring wellbore seal integrity. *Int. J. Greenh. Gas Control* 58, 290–298.
- Gong, Q., Xu, Z.G., Wang, M.Q., Qin, J., 2019a. Numerical investigation on wellbore temperature and pressure during carbon dioxide fracturing. *Appl. Therm. Eng.* 157, 113675.
- Gong, L., Chen, S.C., Zuo, J.Q., Bai, B., Bai, Z., 2019b. Phase prediction of supercritical carbon dioxide and its application in fracturing oil wellbores. *J. Therm. Sci.* 28 (3), 484–493.
- Gou, Y., Zhou, L., Zhao, X., Hou, Z.M., Were, P., 2015. Numerical study on hydraulic fracturing in different types of georeservoirs with consideration of H2M-coupled leak-off effects. *Environ. Earth Sci.* 73 (10), 6019–6034.
- Guo, J.C., Zeng, J., 2015. A coupling model for wellbore transient temperature and pressure of fracturing with supercritical carbon dioxide. *Acta Pet. Sin.* 36 (2), 203–209 (in Chinese).
- Guo, J.C., Zeng, J., Zhang, R., Zhou, C.L., 2015. A dual transient coupling model for wellbore of carbon dioxide injection well. *Acta Pet. Sin.* 36 (8), 976–982 (in Chinese).
- Guo, T.K., Zhang, Y.L., Shen, L., et al., 2022. Numerical study on the law of fracture propagation in supercritical carbon dioxide fracturing. *J. Petrol. Sci. Eng.* 208, 109369.
- Gupta, D., Bobier, D., 1998. The history and success of liquid CO₂ and CO₂/N₂ fracturing system. In: SPE Gas Technology Symposium. Society of Petroleum Engineers Calgary, OnePetro, Calgary, Alberta, Canada, SPE-40016-MS.
- Ha, S.J., Choo, J., Yun, T.S., 2018. Liquid CO₂ fracturing: effect of fluid permeation on the breakdown pressure and cracking behavior. *Rock Mech. Rock Eng.* 51 (11), 3407–3420.
- Haddad, M., Sepehrnoori, K., 2016. XFEM-Based CZM for the simulation of 3D multiple-cluster hydraulic fracturing in quasi-brittle shale formations. *Rock Mech. Rock Eng.* 49 (12), 4731–4748.
- Haris, M., Hou, M.Z., Feng, W.T., Luo, J.S., Zahoor, M.K., Liao, J.X., 2020. Investigative coupled thermo-hydro-mechanical modelling approach for geothermal heat extraction through multistage hydraulic fracturing from hot geothermal sedimentary systems. *Energies* 13 (13), 3504.
- He, Y.T., Yang, Z.Z., Jiang, Y.F., Li, X., Zhang, Y.Q., Song, R., 2020. A full three-dimensional fracture propagation model for supercritical carbon dioxide fracturing. *Energy Sci. Eng.* 8 (8), 2894–2906.
- Heider, Y., 2021. A review on phase-field modeling of hydraulic fracturing. *Eng. Fract. Mech.* 253, 107881.
- Hou, L., Jiang, T.X., Liu, H., et al., 2017. An evaluation method of supercritical CO₂ thickening result for particle transporting. *J. CO₂ Util.* 21, 247–252.
- Huang, Z.W., Zhang, S.K., Yang, R.Y., et al., 2020. A review of liquid nitrogen fracturing technology. *Fuel* 266, 117040.
- Inui, S., Ishida, T., Nagaya, Y., Nara, Y., Chen, Y., Chen, Q., 2014. AE monitoring of hydraulic fracturing experiments in granite blocks using supercritical CO₂, water and viscous oil. In: 48th US Rock Mechanics/Geomechanics Symposium. OnePetro, Minneapolis, MN, USA, ARMA. -2014-7163.
- Isaka, B.A., Ranjith, P., Rathnaweera, T., 2019. The use of super-critical carbon dioxide as the working fluid in enhanced geothermal systems (EGSs): a review study. *Sustain. Energy Techn.* 36, 100547.
- Ishida, T., Aoyagi, K., Niwa, T., et al., 2012. Acoustic emission monitoring of hydraulic fracturing laboratory experiment with supercritical and liquid CO₂. *Geophys. Res. Lett.* 39 (16), L16309.
- Jaimes, M.G., Castillo, R.D., Mendoza, S.A., 2012. High energy gas fracturing: a technique of hydraulic prefracturing to reduce the pressure losses by friction in the near wellbore - a Colombian field application. In: SPE Latin America and Caribbean Petroleum Engineering Conference. OnePetro, Mexico City, Mexico, SPE-152886-MS.
- Jia, Y.Z., Lu, Z.H., Liu, H., Wang, J.H., Cheng, Y.G., Zhang, X.W., 2020. Fracture propagation and morphology due to non-aqueous fracturing: competing roles between fluid characteristics and in situ stress state. *Minerals-Basel.* 10 (5), 428.
- Kasyap, S.S., He, H., Senetakis, K., 2022. 3D DEM analysis of analogue proppant-fractured rock system interaction. *Bull. Eng. Geol. Environ.* 81 (1), 1–15.
- Khan, H.J., Spielman-Sun, E., Jew, A.D., Bargar, J., Kovscek, A., Druhan, J.L., 2021. A critical review of the physicochemical impacts of water chemistry on shale in hydraulic fracturing systems. *Environ. Sci. Technol.* 55 (3), 1377–1394.
- Kresse, O., Weng, X.W., 2018. Numerical modeling of 3D hydraulic fractures interaction in complex naturally fractured formations. *Rock Mech. Rock Eng.* 51 (12), 3863–3881.
- Lecampion, B., Bunger, A., Zhang, X., 2018. Numerical methods for hydraulic fracture propagation: a review of recent trends. *J. Nat. Gas Sci. Eng.* 49, 66–83.
- Lester, Y., Ferrer, I., Thurman, E.M., et al., 2015. Characterization of hydraulic fracturing flowback water in Colorado: implications for water treatment. *Sci. Total Environ.* 512, 637–644.
- Li, X.J., Li, G.S., Wang, H.Z., et al., 2018a. A wellbore flow model and coupling solution for supercritical CO₂ fracturing. *J. China Univ. Pet., Ed. Nat. Sci.* 42 (2), 87–94 (in Chinese).
- Li, T.Y., Razavi, O., Olson, J.E., 2018b. Modeling fracture in layered formations using a simplified 3D displacement discontinuity method. In: 52nd US Rock Mechanics/Geomechanics Symposium. OnePetro, Seattle, Washington, USA. ARMA-2018-1079.
- Li, S.B., Zhang, D.X., 2019. How effective is carbon dioxide as an alternative fracturing fluid? *SPE J.* 24 (2), 857–876.
- Li, M.L., Zhang, F.S., Zhuang, L., Zhang, X., Ranjith, P., 2019a. Micromechanical analysis of hydraulic fracturing in the toughness-dominated regime: implications to supercritical carbon dioxide fracturing. *Comput. Geosci.* 24 (5), 1815–1831.
- Li, X.G., He, Y.T., Huo, M., Yang, Z.Z., Wang, H.Z., Song, R., 2019b. Simulation of coupled thermal-hydro-mechanical processes in fracture propagation of carbon dioxide fracturing in oil shale reservoirs. *Energy Sources Part A* 1–20.
- Li, N.Y., Wang, C., Zhang, S.W., Yu, J.J., Dai, Y.H., 2021a. Recent advances in waterless fracturing technology for the petroleum industry: an overview. *J. Nat. Gas Sci. Eng.* 92, 103999.
- Li, N.Y., Yu, J.J., Wang, C., et al., 2021b. Fracturing technology with carbon dioxide: a review. *J. Petrol. Sci. Eng.* 205, 108793.
- Liao, J.X., Hou, Z.M., Mehmood, F., Feng, W.T., 2019. A 3D approach to study the interaction between hydraulic and natural fracture. *Environ. Earth Sci.* 78 (24), 1–18.

- Liao, J.X., 2020. Development of Coupled THM Models for Reservoir Stimulation and Geo-Energy Production with Supercritical CO₂ as Working Fluid, first ed. Cuvillier Verlag, Gottingen, Germany.
- Liao, J.X., Gou, Y., Feng, W.T., Mehmood, F., Xie, Y.C., Hou, Z.M., 2020a. Development of a full 3D numerical model to investigate the hydraulic fracture propagation under the impact of orthogonal natural fractures. *Acta Geotech* 15 (2), 279–295.
- Liao, J.X., Cao, C., Hou, Z.M., et al., 2020b. Field scale numerical modeling of heat extraction in geothermal reservoir based on fracture network creation with supercritical CO₂ as working fluid. *Environ. Earth Sci.* 79, 1–22.
- Liao, J.X., Hou, Z.M., Haris, M., Tao, Y., Xie, Y.C., Yue, Y., 2020c. Numerical evaluation of hot dry rock reservoir through stimulation and heat extraction using a three-dimensional anisotropic coupled THM model. *Geothermics* 83, 101729.
- Liew, M.S., Danyaro, K.U., Zawawi, N.A.W.A., 2020. A comprehensive guide to different fracturing technologies: a review. *Energies* 13 (13), 3326.
- Lisjak, A., Grasselli, G., 2014. A review of discrete modeling techniques for fracturing processes in discontinuous rock masses. *J. Rock Mech. Geotech.* 6 (4), 301–314.
- Liu, H., Wang, F., Zhang, J., Meng, S.W., Duan, Y.W., 2014. Fracturing with carbon dioxide: application status and development trend. *Petrol. Explor. Dev.* 41 (4), 513–519.
- Liu, L.Y., Zhu, W.C., Wei, C.H., Elsworth, D., Wang, J.H., 2018. Microcrack-based geomechanical modeling of rock-gas interaction during supercritical CO₂ fracturing. *J. Petrol. Sci. Eng.* 164, 91–102.
- Liu, B.L., Suzuki, A., Ito, T., 2020. Numerical analysis of different fracturing mechanisms between supercritical CO₂ and water-based fracturing fluids. *Int. J. Rock Mech. Min.* 132, 104385.
- Luo, Z.F., Zhang, N.L., Zhao, L.Q., et al., 2020. Chemical proppant generated in the fracture from the novel fracturing fluid system. In: SPE Canada Unconventional Resources Conference. OnePetro. Calgary, Alberta, Canada, SPE-200004-MS.
- Luo, Z.F., Wu, L., Zhao, L.Q., Zhang, N.L., Chen, W.H., Liang, C., 2021a. Numerical study on filtration law of supercritical carbon dioxide fracturing in shale gas reservoirs. *Greenhouse Gases: Sci. Technol.* 11 (5), 871–886.
- Luo, Z.F., Cheng, L., Zhao, L.Q., 2021b. Numerical simulation and analysis of complex fracture propagation during SC-CO₂ fracturing using a thermal-hydro-mechanical coupling model. *IOP Conf. Ser. Earth Environ. Sci.* 861 (3), 032013.
- Luo, J.S., Hou, Z.M., Feng, G.Q., Liao, J.X., Haris, M., Xiong, Y., 2022a. Effect of reservoir heterogeneity on CO₂ flooding in tight oil reservoirs. *Energies* 15 (9), 3015.
- Luo, L.N., Kasyap, S.S., He, H., Senetakis, K., 2022b. Laboratory and discrete-based numerical investigation on the collision problem of impactor-block systems with soft-porous and hard-crystalline analog rocks. *Int. J. Numer. Anal. Model.* 46 (3), 594–616.
- Ly, X.R., Zhang, S.C., Yu, B.H., et al., 2015. The wellbore temperature test and simulation analysis for liquid carbon dioxide fracturing management. In: SPE/IATMI Asia Pacific Oil & Gas Conference and Exhibition. OnePetro, Nusa Dua, Bali, Indonesia, SPE-176187-MS.
- Lyu, X.R., Zhang, S.C., Ma, X.F., Wang, F., Mou, J.Y., 2018a. Numerical investigation of wellbore temperature and pressure fields in CO₂ fracturing. *Appl. Therm. Eng.* 132, 760–768.
- Lyu, X.R., Zhang, S.C., Ma, X.F., Wang, F., Mou, J.Y., 2018b. Numerical study of non-isothermal flow and wellbore heat transfer characteristics in CO₂ fracturing. *Energy* 156, 555–568.
- Lyu, X.R., Zhang, S.C., He, Y.Y., Zhuo, Z.H., Zhang, C., Meng, Z., 2021. Numerical investigation on wellbore temperature prediction during the CO₂ fracturing in horizontal wells. *Sustainability-Basel* 13 (10), 5672.
- McAndrew, J., Cisternas, P., Pruvot, A., Kong, X.H., Tong, S.Y., 2017. Water consumption and proppant transport aspects of foam fracturing fluids. In: SPE/AAPG/SEG Unconventional Resources Technology Conference. OnePetro, Austin, Texas, USA, URTEC-2670102-MS.
- Mehmood, F., Hou, M.Z., Liao, J.X., Haris, M., Cao, C., Luo, J.S., 2021. Multiphase multicomponent numerical modeling for hydraulic fracturing with N-Heptane for efficient stimulation in a tight gas reservoir of Germany. *Energies* 14 (11), 3111.
- Memon, S., Feng, R.H., Ali, M., et al., 2022. Supercritical CO₂-shale interaction induced natural fracture closure: implications for scCO₂ hydraulic fracturing in shales. *Fuel* 313, 122682.
- Middleton, R.S., Carey, J.W., Currier, R.P., et al., 2015. Shale gas and non-aqueous fracturing fluids: opportunities and challenges for supercritical CO₂. *Appl. Energy* 147, 500–509.
- Mitu, M., Giurcan, V., Razus, D., Oancea, D., 2017. Inert gas influence on the laminar burning velocity of methane-air mixtures. *J. Hazard Mater.* 321, 440–448.
- Mohammad, P.E., Weichgrebe, D., Cuff, G., Tosarkani, B.M., Rosenwinkel, K.-H., 2018. On-site treatment of flowback and produced water from shale gas hydraulic fracturing: a review and economic evaluation. *Chemosphere* 212, 898–914.
- Mojid, M.R., Negash, B.M., Abdulleh, H., Jufar, S.R., Adewumi, B.K., 2021. A state-of-art review on waterless gas shale fracturing technologies. *J. Petrol. Sci. Eng.* 196, 108048.
- Montgomery, C.T., Smith, M.B., 2010. Hydraulic fracturing: history of an enduring technology. *J. Petrol. Technol.* 62 (12), 26–40.
- Nikolai, P., Rabiyyat, B., Aslan, A., Ilmutdin, A., 2019. Supercritical CO₂: properties and technological applications-A review. *J. Therm. Sci.* 28 (3), 394–430.
- Park, K., Paulino, G.H., 2015. A critical review of traction-separation relationships across fracture surfaces for cohesive zone models of fracture. *Appl. Mech. Rev.* 64 (6), 1002.
- Patankar, N.A., Joseph, D.D., Wang, J., Barree, R.D., Conway, M., Asadi, M., 2002. Power law correlations for sediment transport in pressure driven channel flows. *Int. J. Multiphas. Flow* 28 (8), 1269–1292.
- Peng, P.H., Ju, Y., Wang, Y.L., Wang, S.Q., Gao, F., 2017. Numerical analysis of the effect of natural microcracks on the supercritical CO₂ fracturing crack network of shale rock based on bonded particle models. *Int. J. Numer. Anal. Model.* 41 (18), 1992–2013.
- Potyondy, D., Cundall, P., Lee, C., 1996. Modelling rock using bonded assemblies of circular particles. In: 2nd North American Rock Mechanics Symposium. OnePetro. Canada, Montreal, Quebec, ARMA-96-1937.
- Rwechungula, J.C., Cheng, Y.F., 2021. Numerical analysis to estimate near-wellbore drilling induced failures area for fractured formation using Universal Discrete Element Codes (UDEEC). *Cogent Eng* 8 (1), 1911591.
- Schwartz, M.O., 2016. Modelling the performance of liquefied petroleum gas fracking versus water fracking. *Int. J. Pet. Eng.* 2 (3), 163–181.
- Sihvonen, M., Järvenpää, E., Hietaniemi, V., Huopalahti, R., 1999. Advances in supercritical carbon dioxide technologies. *Trends Food Sci. Technol.* 10 (6–7), 217–222.
- Song, W.Q., Ni, H.J., Wang, R.H., Sun, B.J., Shen, Z.H., 2017. Pressure transmission in the tubing of supercritical carbon dioxide fracturing. *J. CO₂ Util.* 21, 467–472.
- Song, X.Z., Li, G.S., Guo, B., Wang, H.Z., Li, X.J., Lü, Z.H., 2018. Transport feasibility of proppant by supercritical carbon dioxide fracturing in reservoir fractures. *J. Hydrodyn.* 30 (3), 507–513.
- Song, X.H., Guo, Y.T., Zhang, J., et al., 2019. Fracturing with carbon dioxide: from microscopic mechanism to reservoir application. *Joule* 3 (8), 1913–1926.
- Song, W.Q., Ni, H.J., Tang, P., et al., 2021. Simulation of supercritical carbon dioxide fracturing in shale gas reservoir. *J. Therm. Sci.* 30 (4), 1444–1451.
- Span, R., Wagner, W., 1996. A new equation of state for carbon dioxide covering the fluid region from the triple-point temperature to 1100 K at pressures up to 800 MPa. *J. Phys. Chem. Ref. Data* 25 (6), 1509–1596.
- Stormont, J.C., Fernandez, S.G., Taha, M.R., Matteo, E.N., 2018. Gas flow through cement-casing microannuli under varying stress conditions. *Geomech. Energy Environ.* 13, 1–13.
- Sun, B.J., Wang, J.T., Wang, Z.Y., Gao, Y.H., Xu, J.C., 2018. Calculation of proppant-carrying flow in supercritical carbon dioxide fracturing fluid. *J. Petrol. Sci. Eng.* 166, 420–432.
- Suri, Y., Zahidul Islam, S., Hossain, M., 2020. Numerical modelling of proppant transport in hydraulic fractures. *Fluid Dynam. Mater. Process.* 16 (2), 297–337.
- Tang, C.A., 1997. Numerical simulation of progressive rock failure and associated seismicity. *Int. J. Rock Mech. Min.* 34 (2), 249–261.
- Tang, C.A., Tham, L.G., Lee, P.K.K., Yang, T.H., Li, L.C., 2002. Coupled analysis of flow, stress and damage (FSD) in rock failure. *Int. J. Rock Mech. Min.* 39 (4), 477–489.
- Tomac, I., Gutierrez, M., 2017. Coupled hydro-thermo-mechanical modeling of hydraulic fracturing in quasi-brittle rocks using BPM-DEM. *J. Rock Mech. Geotech.* 9 (1), 92–104.
- Wang, H.Z., Li, G.S., Shen, Z.H., 2012. A feasibility analysis on shale gas exploitation with supercritical carbon dioxide. *Energy Sources Part A* 34 (15), 1426–1435.
- Wang, H.Z., Li, G.S., Shen, Z.H., et al., 2015. Experiment on rock breaking with supercritical carbon dioxide jet. *J. Petrol. Sci. Eng.* 127, 305–310.
- Wang, J.T., Sun, B.J., Wang, Z.Y., Zhang, J.B., 2017. Study on filtration patterns of supercritical CO₂ fracturing in unconventional natural gas reservoirs. *Greenhouse Gases: Sci. Technol.* 7 (6), 1126–1140.
- Wang, J.T., Sun, B.J., Li, H., Wang, X., Wang, Z.Y., Sun, X.H., 2018a. Phase state control model of supercritical CO₂ fracturing by temperature control. *Int. J. Heat Mass Tran.* 118, 1012–1021.
- Wang, M., Wang, H., Li, G., Yang, B., Zheng, Y., Lu, Q., 2018b. Numerical study of proppant transport with supercritical CO₂ in fracture. *China Pet. Mach.* 46 (11), 72–78 (in Chinese).
- Wang, H.Z., Wang, M., Yang, B., Lu, Q., Zheng, Y., Zhao, H.Q., 2018c. Numerical study of supercritical CO₂ and proppant transport in different geometrical fractures. *Greenhouse Gases: Sci. Technol.* 8 (5), 898–910.
- Wang, H.Z., Li, X.J., Sepehrmoori, K., Zheng, Y., Yan, W.J., 2019a. Calculation of the wellbore temperature and pressure distribution during supercritical CO₂ fracturing flowback process. *Int. J. Heat Mass Tran.* 139, 10–16.
- Wang, J.T., Wang, Z.Y., Sun, B.J., Gao, Y.H., Wang, X., Fu, W.Q., 2019b. Optimization design of hydraulic parameters for supercritical CO₂ fracturing in unconventional gas reservoir. *Fuel* 235, 795–809.
- Wang, J.H., Elsworth, D., 2020. Fracture penetration and proppant transport in gas-and foam-fracturing. *J. Nat. Gas Sci. Eng.* 77, 103269.
- Wei, C., Cheng, S.Q., Tu, K., et al., 2020. A hybrid analytic solution for a well with a finite-conductivity vertical fracture. *J. Petrol. Sci. Eng.* 188, 106900.
- Wu, L., Zhao, L.Q., Luo, Z.F., Yao, Z.G., 2019. Research progress and prospect on numerical simulation of fracture propagation in SRV fracturing of shale. *Electron. J. Geotech. Eng.* 24, 919–930.
- Wu, L., Luo, Z.F., Zhao, L.Q., Zhang, N.L., Yao, Z.G., Jia, Y.C., 2021. Transient temperature-pressure field model of supercritical CO₂ fracturing wellbore with tubing and annulus co-injection. *Greenhouse Gases: Sci. Technol.* 12 (1), 85–102.
- Wu, L., Luo, Z.F., 2022. Coupled temperature–pressure model of fracture for phase state prediction in supercritical carbon dioxide fracturing. *Energy Sources Part A* 44 (2), 3866–3882.
- Xiao, B., Jiang, T., Zhang, S., 2018. Numerical simulation on proppant transport of liquid carbon dioxide in vertical fracture. *Sci. Technol. Eng.* 18 (12), 186–190 (in Chinese).
- Xiong, Y., Hou, Z.M., Xie, H.P., Zhao, J.Z., Tan, X.C., Luo, J.S., 2022. Microbial-mediated CO₂ methanation and renewable natural gas storage in depleted petroleum reservoirs: a review of biogeochemical mechanism and perspective. *Gondwana Res.* <https://doi.org/10.1016/j.gr.2022.04.017>.

- Xu, J.X., Ding, Y.H., Yang, L.F., et al., 2020. Numerical analysis of proppants transport in tortuous fractures of shale gas reservoirs after shear deformation. *J. Nat. Gas Sci. Eng.* 78, 103285.
- Xue, Y., Liu, J., Ranjith, P.G., Liang, X., Wang, S.H., 2021. Investigation of the influence of gas fracturing on fracturing characteristics of coal mass and gas extraction efficiency based on a multi-physical field model. *J. Petrol. Sci. Eng.* 206, 109018.
- Yan, H., Zhang, J.X., Zhou, N., Li, M., 2019. Staged numerical simulations of supercritical CO₂ fracturing of coal seams based on the extended finite element method. *J. Nat. Gas Sci. Eng.* 65, 275–283.
- Yan, H., Zhang, J.X., Zhou, N., Li, M., Suo, Y., 2020. Numerical simulation of dynamic interactions between two cracks originating from adjacent boreholes in the opposite directions during supercritical CO₂ fracturing coal mass. *Eng. Fract. Mech.* 223, 106745.
- Yan, H., Zhang, J.X., Zhou, N., Wang, Y.B., 2021. Quantitative characterization of crack propagation behavior under the action of stage-by-stage fracturing induced by SC-CO₂ fluid. *Eng. Fract. Mech.* 256, 107984.
- Yang, Z.Z., Yi, L.P., Li, X.G., Chen, Y.T., Sun, J., 2018a. Model for calculating the wellbore temperature and pressure during supercritical carbon dioxide fracturing in a coalbed methane well. *J. CO₂ Util.* 26, 602–611.
- Yang, Z.Z., Yi, L.P., Li, X.G., Han, X.P., Li, Z.C., 2018b. Wellbore temperature and pressure calculation model for supercritical carbon dioxide jet fracturing. *Energy Sources Part A* 41 (2), 185–200.
- Yang, J.F., Ren, Y.Q., Zhang, D.D., Liu, Y.L., Ma, Z., 2021. Numerical simulation of fracturing in coals using water and supercritical carbon dioxide with potential-based cohesive zone models. *Geofluids* 2021, 1–14.
- Yi, L.P., Jia, M., Li, X.G., Yang, Z.Z., 2019. Transient wellbore temperature and pressure calculation model for supercritical CO₂ jet fracturing. *Energy Sources Part A* 43 (11), 1396–1411.
- Zareidarmiyani, A., Salarirad, H., Vilarrasa, V., Kim, K.I., Lee, J., Min, K.B., 2020. Comparison of numerical codes for coupled thermo-hydro-mechanical simulations of fractured media. *J. Rock Mech. Geotech.* 12 (4), 850–865.
- Zhang, X.X., Wang, J.G., Gao, F., Ju, Y., 2017a. Impact of water, nitrogen and CO₂ fracturing fluids on fracturing initiation pressure and flow pattern in anisotropic shale reservoirs. *J. Nat. Gas Sci. Eng.* 45, 291–306.
- Zhang, Y.H., Zhang, Z.K., Sarmadivaleh, M., et al., 2017b. Micro-scale fracturing mechanisms in coal induced by adsorption of supercritical CO₂. *Int. J. Coal Geol.* 175, 40–50.
- Zhang, Q., Ma, D., Wu, Y., Meng, F.F., 2018. Coupled thermal–gas–mechanical (TGM) model of tight sandstone gas wells. *J. Geophys. Eng.* 15 (4), 1743–1752.
- Zhang, Q., Ma, D., Liu, J.F., Wang, J.H., Li, X.B., Zhou, Z.L., 2019. Numerical simulations of fracture propagation in jointed shale reservoirs under CO₂ fracturing. *Geofluids* 1–13, 2019.
- Zhang, W., Wang, C.G., Guo, T.K., et al., 2021a. Study on the cracking mechanism of hydraulic and supercritical CO₂ fracturing in hot dry rock under thermal stress. *Energy* 221, 119886.
- Zhang, Q., Wang, J.H., Gao, Y.F., et al., 2021b. CO₂-Driven hydraulic fracturing trajectories across a preexisting fracture. *Geofluids* 2021, 1–12.
- Zhang, C.P., Liu, S., Ma, Z.Y., Ranjith, P.G., 2021c. Combined micro-proppant and supercritical carbon dioxide (SC-CO₂) fracturing in shale gas reservoirs: a review. *Fuel* 305, 121431.
- Zhang, N.L., Luo, Z.F., Zhao, L.Q., et al., 2022. Innovative thermo-responsive in-situ generated proppant: laboratory tests and field application. *J. Petrol. Sci. Eng.* 208, 109514.
- Zhao, H.Q., Wu, K., Huang, Z.W., Xu, Z.M., Shi, H.Z., Wang, H.Z., 2021. Numerical model of CO₂ fracturing in naturally fractured reservoirs. *Eng. Fract. Mech.* 244.
- Zheng, Y., Wang, H.Z., Yang, B., et al., 2020a. CFD-DEM simulation of proppant transport by supercritical CO₂ in a vertical planar fracture. *J. Nat. Gas Sci. Eng.* 84, 103647.
- Zheng, Y., Wang, H.Z., Shen, Z.H., Yang, B., Tian, G.H., 2020b. CFD simulation of proppant distribution in a vertical fracture during supercritical CO₂ fracturing. In: 54th US Rock Mechanics/Geomechanics Symposium. OnePetro, Golden, Colorado, USA. ARMA-2020-1183.
- Zheng, Y., Wang, H.Z., Li, Y.J., et al., 2021. Effect of proppant pumping schedule on the proppant placement for supercritical CO₂ fracturing. *Petrol. Sci.* 19 (2), 629–638.
- Zhou, L., Hou, Z.M., 2013. A new numerical 3D-model for simulation of hydraulic fracturing in consideration of hydro-mechanical coupling effects. *Int. J. Rock Mech. Min.* 60, 370–380.
- Zhou, L., Hou, Z.M., Gou, Y., Li, M.T., 2014. Numerical investigation of a low-efficient hydraulic fracturing operation in a tight gas reservoir in the North German Basin. *J. Petrol. Sci. Eng.* 120, 119–129.
- Zhou, L., Su, X.P., Hou, Z.M., Lu, Y.Y., Gou, Y., 2016. Numerical investigation of the hydromechanical response of a natural fracture during fluid injection using an efficient sequential coupling model. *Environ. Earth Sci.* 75 (18), 1–17.
- Zhou, Y., Ni, H.J., Shen, Z.H., Wang, M.S., 2020. Study on proppant transport in fractures of supercritical carbon dioxide fracturing. *Energy Fuel* 34 (5), 6186–6196.
- Zhu, W.C., Tang, C.A., 2004. Micromechanical model for simulating the fracture process of rock. *Rock Mech. Rock Eng.* 37 (1), 25–56.
- Zhu, W.C., Wei, C.H., Li, S., Wei, J., Zhang, M.S., 2013. Numerical modeling on distress blasting in coal seam for enhancing gas drainage. *Int. J. Rock Mech. Min.* 59, 179–190.



Prof. Zhengmeng Hou is the head of rock mechanics at Clausthal University of Technology as well as an academician of the Academy of Geosciences and Geotechnologies, Germany. He has been mainly engaged in teaching, scientific research and international cooperation in the fields of unconventional petroleum and geothermal development, hydraulic fracturing, carbon capture utilization and storage, carbon neutrality and energy transition, underground storage of natural gas and strategic oil, especially renewable energy coupled with power-to-X, as well as deep rock mechanics. He has published more than 250 papers included in SCI/El, 10 monographs in English and German and 1 monograph in Chinese, and edited 5 international conference proceedings.